Outage-aware Deployment in Heterogeneous Rayleigh Fading Wireless Sensor Networks

Saeed Karimi-Bidhendi and Hamid Jafarkhani

Abstract

We study a heterogeneous Rayleigh fading wireless sensor network (WSN) in which sensor nodes surveil a field of interest and communicate their sensory data with base stations with the aid of access points as relays. With the goal of improving the energy efficiency of the network, we consider both large-scale and small-scale signal propagation effects in our system model and aim to optimize the node deployment as an effective measure to reduce the wireless communication power consumption of the WSN. We propose a new framework, in which hard deterministic connectivity constraints on communication links are replaced with realistic limitations on outage due to severe stochastic fading. We also consider a radio energy model that reflects the exponential dependence of the transmission power on the rate. We derive the necessary conditions for the optimal deployment that not only minimize the power consumption, but also guarantee all wireless links to have an outage probability below the given threshold. Our theoretical findings are accompanied by simulations that indicate significant performance gains compared to existing node deployment algorithms in the literature.

Index Terms

Deployment, heterogeneous wireless sensor networks, power optimization, outage, Rayleigh fading.

I. Introduction

Wireless sensor networks (WSNs) have attracted widespread attention due to their utilization in numerous applications such as healthcare monitoring [1], surveillance [2], precision agriculture [3], and industrial monitoring [4]. A WSN is mainly comprised of sensor nodes that are deployed inside a field of interest to monitor physical phenomena such as environmental conditions,

Authors are with the Center for Pervasive Communications & Computing, University of California, Irvine, Irvine CA, 92697 USA (e-mail:{skarimib, hamidj}@uci.edu). This work was supported in part by the NSF Award CNS-2229467.

target positions, etc. Each sensor node is equipped with sensing and communication capabilities and can transmit its sensed information back to dedicated base stations (BSs) through wireless communications [5], [6]. Sensor nodes are susceptible to failure due to factors such as adverse environmental conditions and breakdown in the onboard electronics [7]; however, battery power exhaustion remains the major factor causing node failure because sensors operate on batteries that cannot be replaced in most practical applications, especially in hostile regions where sensor nodes are inaccessible [8]. Therefore, energy efficiency is considered the most crucial quality-of-service (QoS) metric for functionality and longevity of WSNs [9]. Among different factors, such as communication, computation, and sensing [10]–[12], that contribute to the network's energy consumption, communication energy has shown to be the dominating factor through empirical studies [13]. Therefore, to preserve the sensor nodes' batteries and increase the WSN's lifetime, access points (APs) are deployed as intermediary nodes to relay the sensory data to BSs.

Improving the energy-efficiency of WSNs has been the center of attention for numerous work in the literature. Many ideas are leveraged for this purpose, such as arranging efficient active and sleep cycles for sensors to preserve their energy [14]–[16] and optimizing the path that sensory data takes to reach BSs [17]–[23]. Among these ideas, optimizing node deployment has been the highlight of many existing work due to its critical role in network's energy consumption and lifetime. This is because the received signal strength is inversely proportional to a power of distance between the transmitter and the receiver; thus, the required transmission energy to guarantee a certain signal-to-noise ratio (SNR) at the receiver node highly depends on the distance and placement of network nodes.

Node deployment algorithms can be categorized in many different ways based on network's setup, node's mobility, hardware characteristics, etc. Some techniques are developed offline and executed in a centralized manner [24] while others are distributed and are based on the assumption that each node has only local information about the state of other nodes [25], [26]. Moreover, several node deployment algorithms are proposed for static networks where nodes are manually deployed at their predetermined locations [27]–[30] while others are curated for mobile networks and calculate the optimal location of nodes based on their respective initial deployment and limited movement energy resources [24], [30], [31]. The optimal deployment highly depends on the homogeneous [19], [32]–[34] or heterogeneous [27]–[30], [35], [36] nature of the WSN. The problem of node deployment in homogeneous WSNs, where nodes have similar hardware characteristics such as storage, computational power, sensitivity, and antenna gain, is

studied in detail [33], [34], [37]. However, these studies do not account for challenges, such as non-convexity and disconnectivity of optimal regions, that arise when network nodes are heterogeneous and have different characteristics. Heterogeneous WSNs have been the subject of study for several recent works [27]–[29]; however, these works along with the majority of similar studies in the literature overlook the real-world properties of the field of interest and do not account for the stochasticity of the communication channel due to the fading process. Another shortcoming of these works is their use of an oversimplified communication energy model in which the exponential dependence of the communication power on the rate is ignored. As a result, these methods underestimate the actual energy consumption of nodes and lead to a network configuration with considerably less reliability and lifetime. This in turn highlights the need for further research and development of models and methods that can realistically reflect the real-world characteristics of WSNs.

The primary motivation and distinguishing characteristics of this work is to address the aforestated shortcomings. We propose a new paradigm in which we move from hard deterministic connectivity constraints on communication links to stochastic schemes with desired low probability of harmful outage. This is because in realistic networks, the transmitted signal can experience severe power degradation before arriving at the receiver node if the communication channel undergoes deep fading; thus, communication links can randomly experience outage due to stochastic nature of the fading process. In our approach, we consider a link connected if its communication channel experiences outage with a probability less than or equal to a desired ϵ value. The choice of ϵ is application specific and in general, a lower ϵ value corresponds to a lower outage probability and a higher chance of connectivity. We study the optimal deployment in heterogeneous Rayleigh fading sensor networks with the aim of minimizing the wireless communication power consumption in such networks. The main contributions of the paper are summarized below:

- Instead of imposing a set of deterministic constraints on communication links, as done in the literature, we consider stochastic constraints that take into account both large-scale path-loss signal attenuation and small-scale signal variation due to Rayleigh fading.
- We consider a radio energy model that takes the heterogeneity of network nodes into account and reflects the exponential dependence of the transmission power on the rate, a shortcoming of the existing work in the literature.
- We provide a detail theoretical analysis of the problem and derive the necessary conditions

of an optimal deployment. Based on the derived necessary conditions of optimality, we propose an alternating optimization algorithm for an energy-efficient node deployment in such networks.

The rest of the paper is organized as follows. The system model and problem formulation are discussed in Section II. In Section III, the optimal deployment in heterogeneous Rayleigh fading WSNs under outage probability constraints on communication channels is studied and an alternating optimization algorithm based on the obtained necessary conditions is provided. Simulation results and concluding remarks are provided in Sections IV and V, respectively.

II. System Model

We consider a heterogeneous WSN that consists of homogeneous sensors, N heterogeneous APs, and M heterogeneous BSs. The field of interest $\Omega \subseteq \mathbb{R}^2$ is a convex polygon including its interior. In particular, each sensor transmits its data to an AP which acts as a relay node and forwards the collected information to BSs. We denote the set of node indices for APs and BSs by $\mathcal{I}_{AP} = \{1, \cdots, N\}$ and $\mathcal{I}_{BS} = \{1, \cdots, M\}$, respectively. While access points and base stations are characterized as a set of $(N+M)$ discrete points within the field of interest, the distribution of densely deployed sensors are described via a continuous and differentiable function $f : \Omega \longrightarrow \mathbb{R}^+$ such that $\int_W f(\omega)d\omega$ is the total number of sensors within the region $W \subseteq \Omega$. In this manuscript, we make the assumption that the prior knowledge of the sensor deployment density $f(\omega)$ is known. For applications such as surveillance, traffic management, and transportation monitoring system that require continuous stream of visual and/or audio data, sensors transmit their sensed information with the bit-rate R_b (bits/s) which is a constant due to sensors' homogeneity [33]. The assumption of constant bit-rate can also be carried out for applications such as environmental temperature and humidity monitoring, where sensors have sporadic activity, by considering time-division multiplexing for sensors' activity. Thus, the total amount of data gathered by sensors within the region W in one time unit is equal to $R_b \int_W f(\omega)d\omega$. Throughout this paper, we assume that each sensor only transmits its data to one AP. Consequently, the field of interest Ω is partitioned into N disjoint regions $\mathbf{W} = (W_1, \cdots, W_N) \subseteq \Omega^N$ such that for each $n \in \mathcal{I}_{AP}$, AP n collects data from sensors within the region $W_n \subseteq \Omega$. For any $n \in \mathcal{I}_{AP}$ and $m \in \mathcal{I}_{BS}$, let $p_n \in \Omega$ and $q_m \in \Omega$ denote the location of AP n and BS m, respectively. In addition, let $\mathbf{P} = (p_1, \cdots, p_N) \in \mathbb{R}^{N\times 2}$ and $\mathbf{Q} = (q_1, \cdots, q_M) \in \mathbb{R}^{M\times 2}$ denote the collective deployment of APs and BSs, respectively.

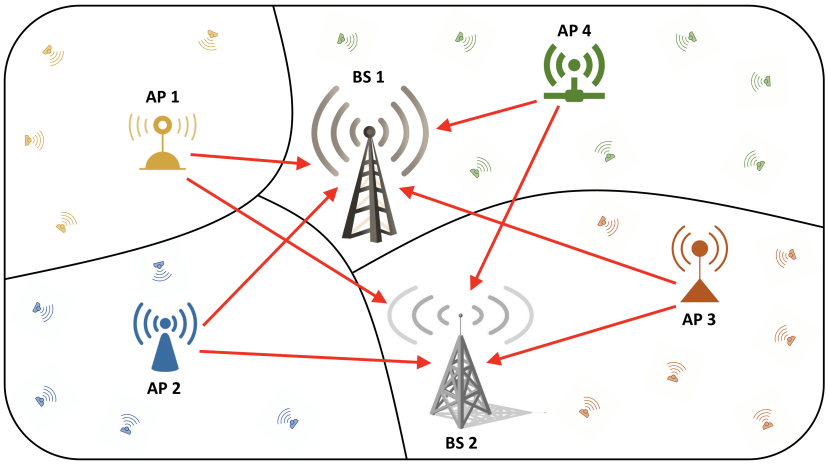

Fig. 1: The system model and network architecture.

In addition to AP deployment $\mathbf{P}$, BS deployment $\mathbf{Q}$, and cell partitioning $\mathbf{W}$, the performance of a WSN heavily depends on the routing protocol by which data is transferred from sensors to base stations. It is important to note that while there may be scenarios where it is appropriate for a sensor to transmit its data directly to the nearby base station, or adhoc scenarios that do not have any hierarchy, in many cases factors such as scalability, network topology, bandwidth, interference reduction, security, and data aggregation favor the use of access points as intermediary nodes. Therefore, in the remaining part of this manuscript, we adopt a routing protocol that involves transmitting data through access points. Our network in this paper can be regarded as a directed bipartite graph where the vertex set can be partitioned into two disjoint subsets containing access points and base stations, respectively, and each edge from AP n to BS m is associated with a non-negative value $F_{n,m}$ (bits/s) denoting the flow of data from AP n to BS m. An example of one such graph is depicted in Fig. 1. Thus, the routing protocol can be characterized by a flow matrix $\mathbf{F} = [F_{n,m}]_{N\times M}$ where $F_{n,m}$ denotes the amount of data transmitted from AP n to BS m in one time unit. Since each AP, say n, transmits all the received data, the in-flow value should be equal to the out-flow value, i.e., $R_b \int_{W_n} f(\omega)d\omega = \sum_{m=1}^{M} F_{n,m}$. Note that instead of directly specifying the flow $F_{n,m}$ from AP n to BS m, we can specify the ratio of out-flow from AP n that goes to BS m, i.e., $r_{n,m} = \frac{F_{n,m}}{\sum_{j=1}^{M} F_{n,j}}$. By definition, it readily follows that $r_{n,m} \in [0, 1]$ and $\sum_{m=1}^{M} r_{n,m} = 1$ since the in-flow to each AP is equal to its out-flow. In particular, the flow matrix $\mathbf{F}$ can be uniquely determined by the cell partitioning $\mathbf{W}$ and the normalized flow matrix $\mathbf{R} = [r_{n,m}]_{N\times M}$.

In this paper, we consider a slow fading channel in which the channel gain is stochastic but remains constant in each frame. We also assume that the receiver can track the fading process, i.e., coherent reception and the transmitter has no knowledge of the channel realization except for its statistical properties. For a channel realization h, the maximum communication rate with arbitrarily small error probability is given by $\log\left(1+|h|^2\gamma\right)$ bits/s/Hz, where γ represents the received signal-to-noise ratio (SNR) due to large-scale propagation effects. The relationship denotes the necessary SNR which, in turn, allows sensors and APs to adjust their transmission power accordingly for a successful data transfer at a given bit-rate and distance. We choose Rayleigh fading for the small-scale propagation because of its applications in rich scattering non-line-of-sight WSN environments although our general approach is independent of the distribution and works for other channel statistics. For a Rayleigh fading channel, the small-scale channel distribution is a standard complex normal random variable, i.e., $h \sim \mathcal{CN}(0,1)$; therefore, $|h|^2$ has an exponential distribution with parameter 1. Due to stochasticity of the channel realization, the decoding error probability cannot become arbitrarily small regardless of the code used by the transmitter [38]. Hence, the primary objective in this paper is to find an optimal deployment that minimizes the wireless transmission power consumption of the WSN subject to a given outage probability threshold. For a given data flow $F_{n,m}$, the outage probability is given by [38]:

$$p_{\text{out}_{n,m}}\left(F_{n,m}\right)=\mathbb{P}\Big\{B\log\left(1+|h|^2\gamma_{n,m}\right)<F_{n,m}\Big\}. \tag{1}$$

Similarly, the outage probability for the link between a sensor located at $\omega\in\Omega$ and AP n is:

$$p_{\text{out}_{\omega,n}}\left(R_b\right)=\mathbb{P}\Big\{B\log\left(1+|h|^2\gamma_{\omega,n}\right)<R_b\Big\}. \tag{2}$$

The received SNR is proportional to the transmit power, i.e., $\gamma \propto P_t \times d^{-\alpha}$ where d is the distance between the transmitter and receiver, and $2\leq\alpha\leq 5$ is the large-scale path loss exponent [39]. We consider the Friis free space loss equation, i.e., $\alpha=2$. More precisely, if AP n sends a signal with transmission power $P^{(n,m)}_{\text{transmit}}$, the received signal power at BS m, i.e., $P^{(n,m)}_{\text{receive}}$, is

$$P^{(n,m)}_{\text{receive}}=P^{(n,m)}_{\text{transmit}}\times\frac{G_{t_n}G_{r_m}\lambda_c^2}{(4\pi)^2\left\|p_n-q_m\right\|^2L_n}, \tag{3}$$

where G_{t_n} is the transmitter antenna gain of AP n, G_{r_m} is the receiver antenna gain of BS m, λ_c is the wavelength of the carrier signal, and L_n denotes all other losses that are not related to the propagation loss such as loss at the antennas, filters, transmission line attenuation, etc. [40].

Therefore, for the spectral noise density of σ Watts/Hz, the received SNR $\gamma_{n,m}$ is given by:

$$\gamma_{n,m} = \frac{P^{(n,m)}_{\text{receive}}}{\sigma B} = P^{(n,m)}_{\text{transmit}} \times \frac{G_{t_n} G_{r_m} \lambda_c^2}{\sigma B \left(4\pi\right)^2 \|p_n - q_m\|^2 L_n}. \tag{4}$$

Similarly, for a sensor located at $\omega \in \Omega$, sending a signal with transmission signal power $P^{(\omega,n)}_{\text{transmit}}$, the received SNR $\gamma_{\omega,n}$ at AP n is given by:

$$\gamma_{\omega,n} = \frac{P^{(\omega,n)}_{\text{receive}}}{\sigma B} = P^{(\omega,n)}_{\text{transmit}} \times \frac{G_{t_{\text{sensor}}} G_{r_n} \lambda_c^2}{\sigma B \left(4\pi\right)^2 \|p_n - \omega\|^2 L_{\text{sensor}}}, \tag{5}$$

where $G_{t_{\text{sensor}}}$ and L_{sensor} are the common transmitter antenna gain and system loss of the homogeneous sensors, respectively. For a given outage probability threshold of ϵ, our goal is to find the optimal WSN deployment that minimizes the total wireless transmission power consumption of the network subject to all channels having an outage probability of less than or equal to ϵ. Thus, the network's weighted communication power consumption can be written as:

$$\mathcal{P}\left(\mathbf{P}, \mathbf{Q}, \mathbf{W}, \mathbf{R}\right) = \sum_{n=1}^{N} \int_{W_n} P^{(\omega,n)}_{\text{transmit}} f(\omega) d\omega + \lambda \sum_{n=1}^{N} \sum_{m=1}^{M} P^{(n,m)}_{\text{transmit}} \tag{6}$$

$$\text{s.t.} \quad p_{\text{out}_{n,m}}\left(F_{n,m}\right) \leq \epsilon \quad \text{and} \quad p_{\text{out}_{\omega,n}}\left(R_b\right) \leq \epsilon, \qquad \forall n \in \mathcal{I}_{AP},\ m \in \mathcal{I}_{BS}, \tag{7}$$

where the Lagrangian multiplier $\lambda \geq 0$ provides a trade-off between the sensor transmission power $\sum_{n=1}^{N} \int_{W_n} P^{(\omega,n)}_{\text{transmit}} f(\omega) d\omega$ and AP transmission power $\sum_{n=1}^{N} \sum_{m=1}^{M} P^{(n,m)}_{\text{transmit}}$. Our goal is to minimize the constrained objective function in Eqs. (6) and (7) over node deployments $\mathbf{P}$ and $\mathbf{Q}$, cell partitioning $\mathbf{W}$, and normalized flow matrix $\mathbf{R}$, which is the subject of the next section.

III. Optimal Deployment under Outage Probability Constraint

In this section, we focus on our primary objective function and aim to minimize the wireless power consumption $\mathcal{P}$ in Eq. (6) subject to outage probability constraints given in Eq. (7). Our goal is to find the optimal deployment $\mathbf{P}^* = (p_1^*, \cdots, p_N^*)$ and $\mathbf{Q}^* = (q_1^*, \cdots, q_M^*)$, cell partitioning $\mathbf{W}^* = (W_1^*, \cdots, W_N^*)$, and the normalized flow matrix $\mathbf{R}^* = \left[r_{n,m}^*\right]_{N \times M}$ that minimize the wireless transmission power consumption of the network. Note that the optimal value for each of the four variables $\mathbf{P}$, $\mathbf{Q}$, $\mathbf{W}$, and $\mathbf{R}$ depends on the value of the other three and this optimization problem is NP-hard. Our aim is to derive the necessary conditions of optimality and devise an algorithm that iteratively optimizes the value of each variable while the other variables are held fixed. We accomplish this goal in the following three steps:

Step 1 [optimizing P and Q while W and R are fixed]: First, we rewrite the objective function $\mathcal{P}$ according to the constraints given in Eq. (7). For a wireless link with flow $F_{n,m}$ from AP n to BS m, we have[1]:

$$\mathbb{P}\left\{|h|^2 < \frac{2^{\frac{F_{n,m}}{B}}-1}{\gamma_{n,m}}\right\} \leq \epsilon \qquad \Longrightarrow \qquad \gamma_{n,m} \geq \frac{2^{\frac{F_{n,m}}{B}}-1}{\ln\left(\frac{1}{1-\epsilon}\right)}, \tag{8}$$

where the right-hand-side inequality follows from the exponential distribution of $|h|^2$. Using Eq. (4), we can rewrite Eq. (8) as

$$P_{\text{transmit}}^{(n,m)} \geq \frac{\sigma B\,(4\pi)^2\, L_n \|p_n - q_m\|^2 \left(2^{\frac{F_{n,m}}{B}}-1\right)}{G_{t_n} G_{r_m} \lambda_c^2 \times \ln\left(\frac{1}{1-\epsilon}\right)} = \frac{b_{n,m}}{\ln\left(\frac{1}{1-\epsilon}\right)} \|p_n - q_m\|^2 \times \left(2^{\frac{F_{n,m}}{B}}-1\right), \tag{9}$$

where $b_{n,m} = \frac{\sigma B \times (4\pi)^2 \times L_n}{G_{t_n} \times G_{r_m} \times \lambda_c^2}$. Hence, Eq. (9) yields a lower bound on the required transmission power at AP n that guarantees an outage probability no greater than ϵ at the corresponding base station. Note that the minimum transmission power occurs when $P_{\text{transmit}}^{(n,m)}$ is equal to its lower bound in Eq. (9) which corresponds to having an outage probability of $p_{\text{out}_{n,m}}(F_{n,m}) = \epsilon$. Similarly, for a sensor located at ω that transmits its data to AP n, we have:

$$P_{\text{transmit}}^{(\omega,n)} \geq \frac{\sigma B\,(4\pi)^2\, L_{\text{sensor}} \times \|p_n - \omega\|^2 \times \left(2^{\frac{R_b}{B}}-1\right)}{G_{t_{\text{sensor}}} G_{r_n} \lambda_c^2 \times \ln\left(\frac{1}{1-\epsilon}\right)} = \frac{a_n}{\ln\left(\frac{1}{1-\epsilon}\right)} \|p_n - \omega\|^2 \left(2^{\frac{R_b}{B}}-1\right), \tag{10}$$

where $a_n = \frac{\sigma B \times (4\pi)^2 \times L_{\text{sensor}}}{G_{t_{\text{sensor}}} \times G_{r_n} \times \lambda_c^2}$. Using Eqs. (9) and (10), we can rewrite the objective function $\mathcal{P}$ in Eq. (6) as follows:

$$\mathcal{P}(\mathbf{P}, \mathbf{Q}, \mathbf{W}, \mathbf{R}) = \sum_{n=1}^{N} \int_{W_n} \frac{a_n}{\ln\left(\frac{1}{1-\epsilon}\right)} \|p_n - \omega\|^2 \left(2^{\frac{R_b}{B}}-1\right) f(\omega) d\omega$$

[1]By implementing a Time Division Multiple Access (TDMA) protocol at the network's access point layer, we can minimize the impact of interference caused by simultaneous transmissions to base stations. This effectively prevents a significant decrease in the received SINR and enables efficient communication between multiple access points and the same base station. At the sensor layer of the network, two types of interference can occur: intra-region interference and inter-region interference. To address intra-region interference, a TDMA scheduling scheme can be devised to allocate non-overlapping time slots to different sensors within the same region, thus reducing such interference. As for inter-region interference, established methods for managing co-channel interference in cellular networks can be utilized. A common approach, which we also employ, involves implementing fixed frequency re-use patterns [41]. This method aims to minimize inter-region interference while maximizing the efficient utilization of the available frequency bandwidth by assigning the same radio frequencies to regions that are significantly distant from each other. It is important to note that more sophisticated techniques such as advanced MAC protocols, OFDMA, Space Division Multiple Access (SDMA) methods, decoding and re-transmission schemes, and others can further enhance the network's interference management capabilities. However, our framework, methodology, and algorithm remain independent of the specific physical layer or higher layer networking solutions employed, as long as they ensure interference avoidance within the network and maintain the logarithmic relationship between the power and the rate. Therefore, while assuming higher-level coordination for interference mitigation in the rest of this manuscript, the design of specific protocols depends on the application and falls beyond the manuscript's scope.

$$+\lambda\sum_{n=1}^{N}\sum_{m=1}^{M}\frac{b_{n,m}}{\ln\left(\frac{1}{1-\epsilon}\right)}\|p_n-q_m\|^2\Big(2^{\frac{F_{n,m}}{B}}-1\Big). \tag{11}$$

The objective function $\mathcal{P}$ in Eq. (11) incorporates the $\epsilon-$threshold constraints on outage probabilities, which were previously expressed as Eq. (7). These constraints are now included as a constant factor $\frac{1}{\ln\left(\frac{1}{1-\epsilon}\right)}$ within the objective function.

The Lagrangian dual equivalent of the objective function described in Eq. (11) minimizes the total sensor powers while imposing a constraint on the total power consumption of access points. Equivalently, one can minimize the total power consumption of access points while forcing a constraint on the total sensor powers. Both scenarios will result in the same tradeoffs as shown in Fig. 5. In addition, it is important to highlight that the total power constraint can be modified to incorporate specific individual power constraints. This can be achieved by introducing separate Lagrangian multipliers for each access point.

Now, for a fixed $\mathbf{W}$ and $\mathbf{R}$, the optimal deployment is given by the following proposition.

Proposition 1: The necessary conditions for the optimal AP and BS deployments $\mathbf{P}^*$ and $\mathbf{Q}^*$ in a heterogeneous WSN with the wireless transmission power consumption defined in Eq. (6) and the outage probability constraint ϵ on all wireless links are given by:

$$p_n^*=\frac{a_n\Big(2^{\frac{R_b}{B}}-1\Big)v_nc_n+\lambda\sum_{m=1}^{M}b_{n,m}\Big(2^{\frac{F_{n,m}}{B}}-1\Big)q_m^*}{a_n\Big(2^{\frac{R_b}{B}}-1\Big)v_n+\lambda\sum_{m=1}^{M}b_{n,m}\Big(2^{\frac{F_{n,m}}{B}}-1\Big)}, \qquad \forall n\in\mathcal{I}_{AP}, \tag{12}$$

$$q_m^*=\frac{\sum_{n=1}^{N}b_{n,m}\Big(2^{\frac{F_{n,m}}{B}}-1\Big)p_n^*}{\sum_{n=1}^{N}b_{n,m}\Big(2^{\frac{F_{n,m}}{B}}-1\Big)}, \qquad \forall m\in\mathcal{I}_{BS}, \tag{13}$$

where $v_n=\int_{W_n}f(\omega)d\omega$ and $c_n=\frac{\int_{W_n}\omega f(\omega)d\omega}{\int_{W_n}f(\omega)d\omega}$ are the volume and centroid of the region W_n, respectively. The proof of Proposition 1 is provided in Appendix A.

Step 2 [optimizing $\mathbf{W}$ while $\mathbf{P}$, $\mathbf{Q}$, and $\mathbf{R}$ are fixed]: First, we study the properties of region boundaries in an optimal cell partitioning $\mathbf{W}^*$. Note that while $\mathbf{F}$ can be uniquely determined by $\mathbf{W}$ and $\mathbf{R}$, it only depends on the region volumes and not their actual geometric shape. More precisely, if we let $V=(v_1,\cdots,v_N)$ where v_n is the volume of region W_n, then $\mathbf{F}$ can be uniquely calculated by V and $\mathbf{R}$ as well. Therefore, Eq. (11) indicates that APs' transmission power only depends on the region volumes and not their geometrical shape. In other words, we can manipulate region boundaries to reduce the sensors' power consumption in Eq. (11) and by extension the total power consumption $\mathcal{P}$ since by keeping the region volumes fixed, APs'

power consumption remains unchanged. Using this intuition, we have:

Lemma 1: Let $\mathbf{W}^* = (W_1^*, \cdots, W_N^*)$ be an optimal cell partitioning that minimizes the constrained objective function $\mathcal{P}$ in Eqs. (6) and (7) for a given node deployment and data routing. Let $\delta_{i,j}^* = W_i^* \cap W_j^*$ be the boundary between neighboring regions W_i^* and W_j^*. Then, $\delta_{i,j}^*$ is either a segment perpendicular to the line $\overline{p_i p_j}$ if $a_i = a_j$ or an arc with its center placed at $c = \frac{a_i p_i - a_j p_j}{a_i - a_j}$ if $a_i \neq a_j$.

The proof of Lemma 1 is provided in Appendix B.

Let $h_{i,j}^*$ be the intersection point between the optimal boundary $\delta_{i,j}^*$ and the segment $\overline{p_i p_j}$ in Lemma 1. The following proposition provides the necessary condition on the location of $h_{i,j}^*$.

Proposition 2: Let $\mathbf{W}^* = (W_1^*, \cdots, W_N^*)$ be an optimal cell partitioning that minimizes the constrained objective function $\mathcal{P}$ in Eqs. (6) and (7) for a given node deployment $\mathbf{P}$, $\mathbf{Q}$, and data routing $\mathbf{R}$. Let $\delta_{i,j}^* = W_i^* \cap W_j^*$ be the boundary between neighboring regions W_i^* and W_j^* which intersects the line $\overline{p_i p_j}$ at point $h_{i,j}^*$. Then, we have

$$\begin{aligned} & a_i \left\| p_i - h_{i,j}^* \right\|^2 \left(2^{\frac{R_b}{B}} - 1 \right) + \lambda \sum_{t=1}^{M} \frac{\ln(2)}{B} \times R_b \times r_{i,t} \times b_{i,t} \left\| p_i - q_t \right\|^2 \times 2^{\frac{r_{i,t} R_b v_i^*}{B}} \\ = & a_j \left\| p_j - h_{i,j}^* \right\|^2 \left(2^{\frac{R_b}{B}} - 1 \right) + \lambda \sum_{t=1}^{M} \frac{\ln(2)}{B} \times R_b \times r_{j,t} \times b_{j,t} \left\| p_j - q_t \right\|^2 \times 2^{\frac{r_{j,t} R_b v_j^*}{B}}. \end{aligned} \tag{14}$$

The proof of Proposition 2 is provided in Appendix C.

Step 3 [optimizing $\mathbf{R}$ while $\mathbf{P}$, $\mathbf{Q}$, and $\mathbf{W}$ are fixed]: Note that for a given deployment $\mathbf{P}$, $\mathbf{Q}$, and cell partitioning $\mathbf{W}$, the sensor power consumption is fixed and $\mathbf{R}$ only affects the AP power consumption in Eq. (11). Since the cell partitioning $\mathbf{W}$ is fixed and each AP directly transmits its data to base stations, the optimization problem can be split into N objective functions, one for each AP, and they can be optimized separately. More specifically, for AP n, we need to optimize the following objective function

$$\underset{F_{n,1} \cdots F_{n,M}}{\arg\min} \sum_{m=1}^{M} \frac{b_{n,m}}{\ln\left(\frac{1}{1-\epsilon}\right)} \left\| p_n - q_m \right\|^2 \times \left(2^{\frac{F_{n,m}}{B}} - 1 \right), \tag{15}$$

$$\text{s.t.} \sum_{m=1}^{M} F_{n,m} = \int_{W_n} R_b f(\omega) d\omega = R_b v_n \quad , \quad F_{n,m} \geq 0 \text{ for all } m \in \mathcal{I}_{BS}. \tag{16}$$

Note that when the sum of exponents is fixed, the minimum of the sum of exponentials with the same base occurs when all exponents are equal. For instance, if for three variables x, y, and z we have $x+y+z = c$, then the minimum of $2^x + 2^y + 2^z$ occurs when $x = y = z = \frac{c}{3}$. Using this

Algorithm 1: Optimal routing in heterogeneous WSNs with outage probability constraint

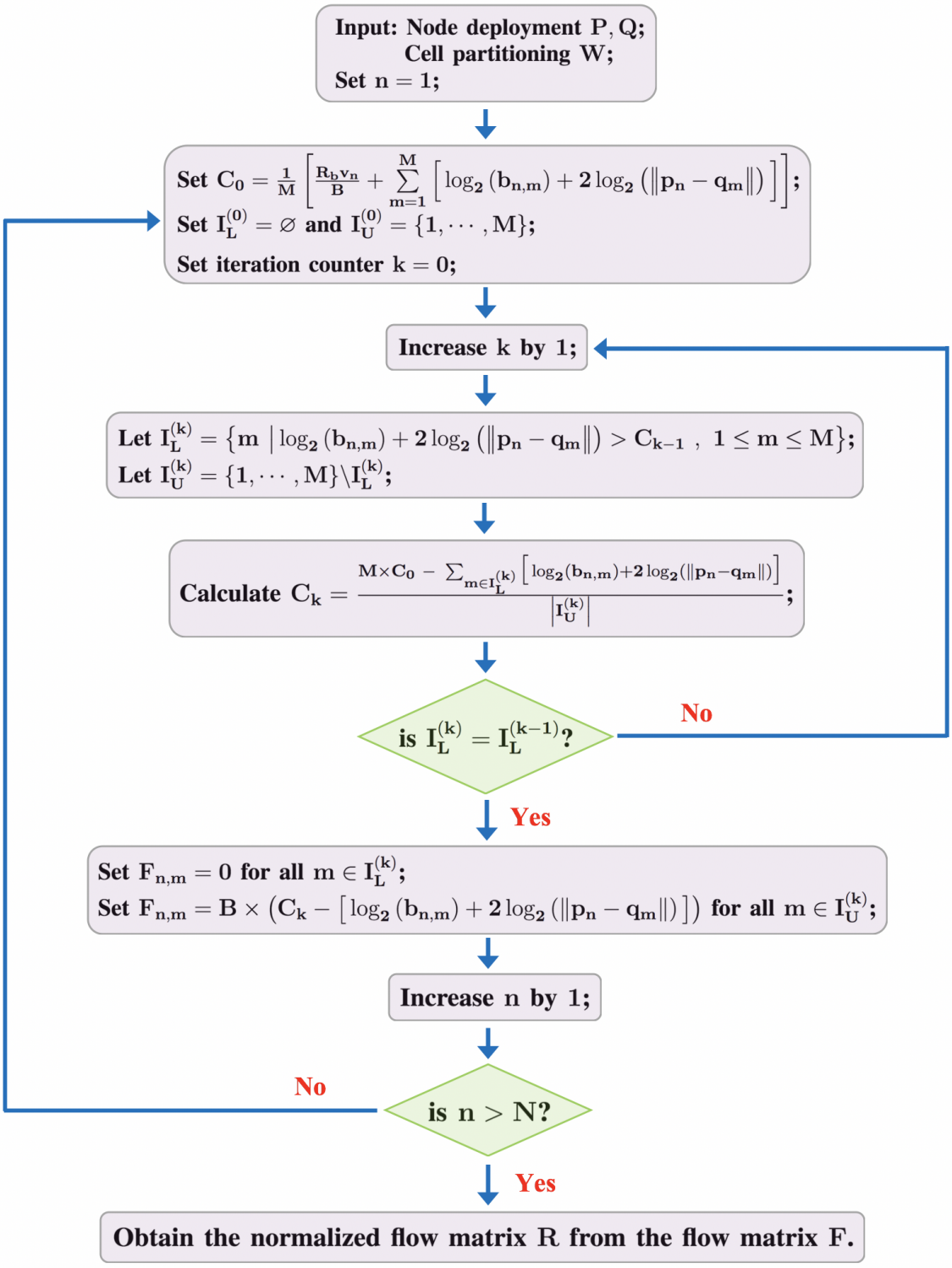

intuition and the fact that all elements of the flow matrix are non-negative, we propose Algorithm 1 that yields the optimal solution of the constrained optimization problem in Eqs. (15)-(16) for

each AP n. Note that once the optimal flow matrix $\mathbf{F}^*$ is obtained, the corresponding normalized flow matrix $\mathbf{R}^*$ can be calculated from the definition.

Algorithm 2: Power-Optimized Outage-aware Lloyd Algorithm

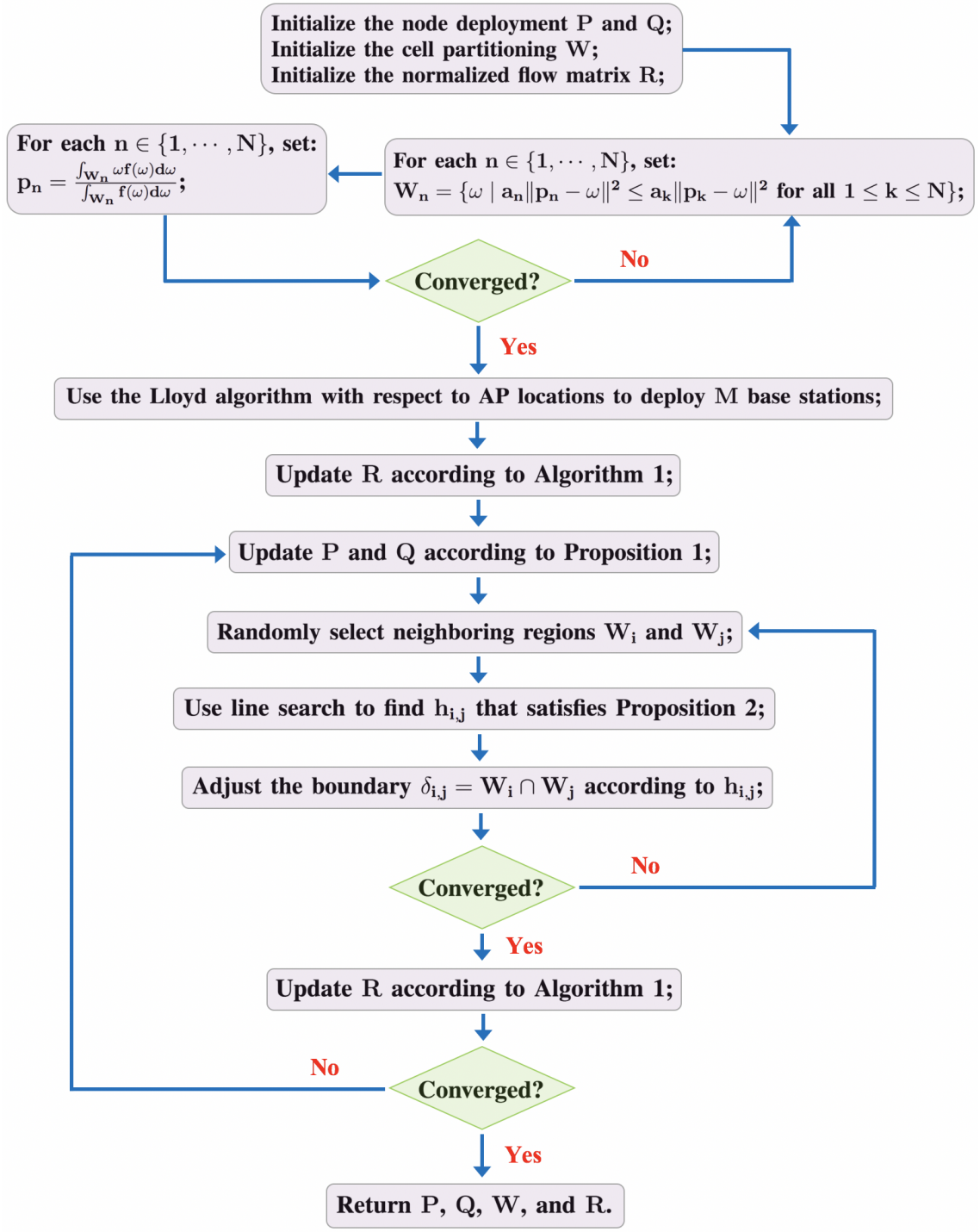

Proposition 3: For a given node deployment $\mathbf{P}$, $\mathbf{Q}$, and cell partitioning $\mathbf{W}$, Algorithm 1 yields

the optimal normalized flow matrix $\mathbf{R}^* = \arg\min_{\mathbf{R}} \mathcal{P}(\mathbf{P}, \mathbf{Q}, \mathbf{W}, \mathbf{R})$ for the heterogeneous WSN under the outage probability constraints in Eq. (7).

The proof of Proposition 3 is provided in Appendix D.

Now, inspired by the Lloyd Algorithm [41], we propose Algorithm 2, named Power-Optimized Outage-aware Lloyd (POOL) Algorithm, to optimize node deployment, cell partitioning, and data routing in our heterogeneous WSN and minimize the wireless communication power consumption in Eq. (6) under outage probability constraints given in Eq. (7).

Proposition 4: The POOL algorithm is an iterative improvement algorithm, i.e., the objective function $\mathcal{P}$ is non-increasing and the algorithm converges.

The proof of Proposition 4 is provided in Appendix E.

We conclude this section by analyzing the complexity of the POOL algorithm. Let's denote the maximum number of iterations for the three convergence criteria in the POOL algorithm as T_1, T_2, and T_3 respectively. Additionally, let L represent the maximum number of points to consider in the line search. The initial loop in the POOL algorithm performs N operations per iteration, and the maximum number of iterations is T_1. Hence, its complexity can be expressed as $\mathcal{O}(T_1 N)$. The subsequent Lloyd algorithm has a computational complexity of $\mathcal{O}(MN)$ for a fixed number of iterations. The inner loop of Algorithm 1 repeats at most M times. Consequently, updating $\mathbf{R}$ according to Algorithm 1 requires $\mathcal{O}(MN)$ operations. Updating $\mathbf{P}$ and $\mathbf{Q}$ using Equations (12) and (13) also involves $\mathcal{O}(MN)$ operations. Each point in the line search has a complexity of $\mathcal{O}(M)$. The complexity of $\mathcal{O}(T_2 LM)$ arises when we take into account the maximum of L points and T_2 pairs of randomly selected neighboring regions. The procedure continues by updating the data routing $\mathbf{R}$ using Algorithm 1 and repeating the outer loop for a maximum of T_3 iterations. Consequently, the overall computational complexity can be expressed as $\mathcal{O}\big(T_1 N + MN + MN + T_3(MN + T_2 LM + MN)\big)$, or simply $\mathcal{O}(MN)$ in terms of the number of access points and base stations.

IV. Experiments

Simulations are performed for a heterogeneous Rayleigh fading sensor network consisting of 15 APs, 3 BSs, and 1000 sensors. The field of interest Ω is a square area of size $10\text{km} \times 10\text{km}$. The bit-rate and the carrier wavelength are set to $R_b = 30\text{Kbps}$ and $\lambda_c = 3\text{m}$, respectively. We consider no system loss, i.e., $L_{\text{sensor}} = L_n = 1$ for all $n \in \mathcal{I}_{AP}$, and a transmitter antenna gain of $G_{t_{\text{sensor}}} = 1$ for all homogeneous sensors. We denote the transmitter and receiver antenna gains

of AP n by $G_{t_n}^{(\text{AP})}$ and $G_{r_n}^{(\text{AP})}$, respectively, and the receiver antenna gain of BS m by $G_{r_m}^{(\text{BS})}$. Let us denote $\mathcal{S}_1 = \{1, 2, 3, 4, 8, 9, 10\}$, $\mathcal{S}_2 = \{1, 2, 5, 6, 8, 9, 12, 13\}$, and $\mathcal{S}_3 = \{1, 2\}$. These indices are generated at random to ensure fairness and avoid any biased preference towards specific antenna gain values. Then, we set

$$G_{t_n}^{(\text{AP})} = \begin{cases} 2 & \text{if } n \in \mathcal{S}_1 \\ 4 & \text{otherwise} \end{cases}, \quad G_{r_n}^{(\text{AP})} = \begin{cases} 2 & \text{if } n \in \mathcal{S}_2 \\ 4 & \text{otherwise} \end{cases}, \quad G_{r_m}^{(\text{BS})} = \begin{cases} 2 & \text{if } m \in \mathcal{S}_3 \\ 4 & \text{otherwise.} \end{cases} \tag{17}$$

We assume that all communication channels have a spectral width of $B = 500$KHz and a spectral noise density of $\sigma = 2 \times 10^{-17}$ Watts/Hz. Note that the parameters a_n and $b_{n,m}$ can be calculated from the experimental setup that is outlined above. For instance, we have $b_{6,2} = \frac{\sigma B \times (4\pi)^2 \times L_6}{G_{t_6}^{(\text{AP})} \times G_{r_2}^{(\text{BS})} \times \lambda_c^2} \simeq 2.19 \times 10^{-11}$ Watts/m^2. We restrict all wireless links to have an outage probability less than or equal to $\epsilon = 1\%$. Note that the choice of the Lagrangian multiplier λ is application specific and it encodes the priority level of minimizing the AP power consumption over the sensor power consumption in $\mathcal{P}$. In particular, larger λ corresponds to higher priority of minimizing the AP power consumption for the constrained objective function in Eqs. (6) and (7). Here, we set $\lambda = 0.25$, which is less than one, to encode the preference that minimizing the sensor power consumption has higher priority over the AP power consumption. Later on, we illustrate how to systematically select λ for an exemplary application requirement. Finally, we conduct the experiments for two sensor density functions: (1) Uniform PDF; and (2) Gaussian mixture PDF given as:

$$\begin{aligned} f(\omega) = &\frac{1}{2} \times \mathcal{N}\left(\begin{bmatrix} 3 \times 10^3 \\ 3 \times 10^3 \end{bmatrix}, \begin{bmatrix} 1.5 \times 10^6 & 0 \\ 0 & 1.5 \times 10^6 \end{bmatrix} \right) \\ &+ \frac{1}{4} \times \mathcal{N}\left(\begin{bmatrix} 6 \times 10^3 \\ 7 \times 10^3 \end{bmatrix}, \begin{bmatrix} 2 \times 10^6 & 0 \\ 0 & 2 \times 10^6 \end{bmatrix} \right) \\ &+ \frac{1}{4} \times \mathcal{N}\left(\begin{bmatrix} 7.5 \times 10^3 \\ 2.5 \times 10^3 \end{bmatrix}, \begin{bmatrix} 10^6 & 0 \\ 0 & 10^6 \end{bmatrix} \right). \end{aligned}$$

We compare our proposed POOL Algorithm with cluster formation (CF) Algorithm [42], Genetic Algorithm (GA) [43], heterogeneous two-tier Lloyd (HTTL) Algorithm [27], particle swarm optimization (PSO) Algorithm [44], and virtual force Algorithm (VFA) [45]. The main motivation behind choosing these methods for comparison purposes is that they represent state-

TABLE I: Weighted power comparison between different methods ($\mathcal{P}$)

Method	CF	GA	HTTL	**POOL**	PSO	VFA
Weighted Power (W) for the uniform PDF	3.57	1.75	1.27	**0.59**	2.93	1.95
Weighted Power (W) for the Gaussian mixture PDF	7.74	2.76	1.18	**0.50**	2.04	3.65

of-the-art node deployment methods in different strategy categories. The CF algorithm falls within the category of methods that take a graph-theoretic approach for load balancing and energy efficiency. The Genetic Algorithm belongs to the category of evolutionary algorithms and employs optimization techniques inspired by biology, utilizing operations such as mutation, crossover, and selection. The HTTL algorithm belongs to the family of geometric-based methods in which the field of interest is partitioned into several regions, one for each network node, based on a predefined measure of closeness. The PSO algorithm represents the class of meta-heuristic node deployment techniques in which optimization tools are used to find optimal node positions. Finally, VFA is a prominent example of force-based techniques and has inspired numerous methods that achieve optimal deployment by applying virtual forces to relocate nodes. For all these algorithms, the final deployment and the resulting weighted power consumption value depend on the initial deployment from which these algorithms start. Hence, except for our POOL algorithm which is run only once, we run other methods ten times (corresponding to ten different random initial deployments) and report the one that yields the best weighted power consumption.

Table I summarizes the weighted transmission power consumption of the heterogeneous WSN outlined above for the CF, GA, HTTL, POOL, PSO, and VFA algorithms. For the uniform and Gaussian mixture sensor distributions, the POOL algorithm leads to weighted power consumption values of 590mW and 496mW, respectively, and outperforms all other methods. Notably, the POOL algorithm achieves a power consumption value that is less than half of the second best algorithm, i.e., the HTTL algorithm, which in turn leads to a more sustainable WSN architecture. The final node deployment for uniform and Gaussian mixture sensor distributions are shown in Figs. 2 and 3, respectively, where APs are denoted by red squares and BSs are depicted by black circles. Areas for which the sensory data ends up in the same BS are shown using the same color. Note that in Figs. 2c and 3c, some regions are split into two or three colors since, following the optimal routing protocol in Algorithm 1, the corresponding APs are transmitting

to multiple BSs instead of a single BS.

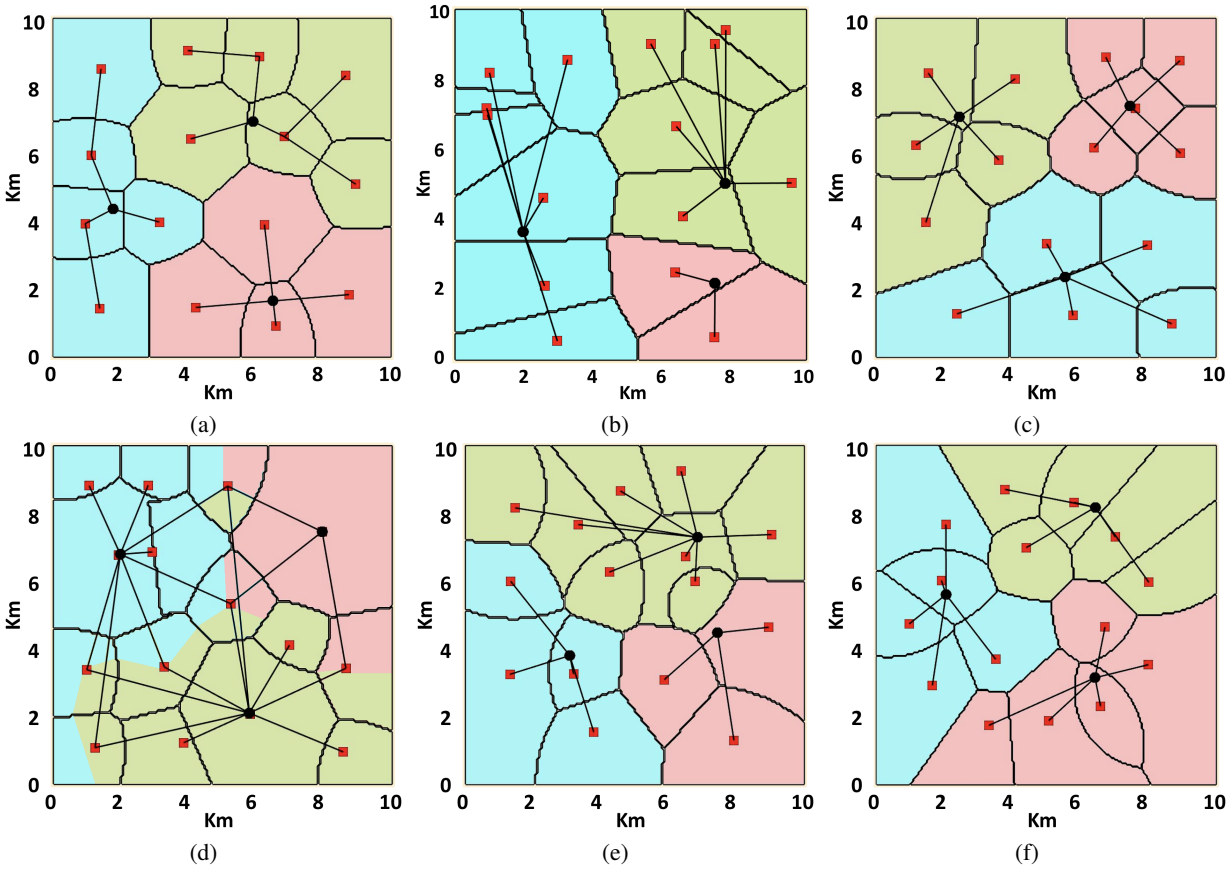

Fig. 2: Node deployment for uniform PDF. (a) CF (b) GA (c) HTTL (d) POOL (e) PSO (f) VFA.

Some key factors contributing to the superior performance of the POOL algorithm are worth noting: While according to the Shannon's capacity formula, the required SNR for an error-free information transmission grows exponentially with the required bit-rate, most methods in the literature consider a linear approximation to this exponential behavior. Such a linear approximation results in an underestimation of the actual power consumption and a network configuration that is suboptimal and consumes higher power when evaluated based on the network's actual power consumption. In contrast, our approach in this work takes the exponential relationship between SNR and bit-rate into account. Another contributing factor is that this exponential relationship between the required transmission power and the flow of data is exploited in finding the optimal routing for data transfer in Algorithm 1 using Lemma 3.

Designing a wireless sensor network necessitates careful consideration of several factors to ensure optimal performance. One crucial aspect is determining the number of APs required

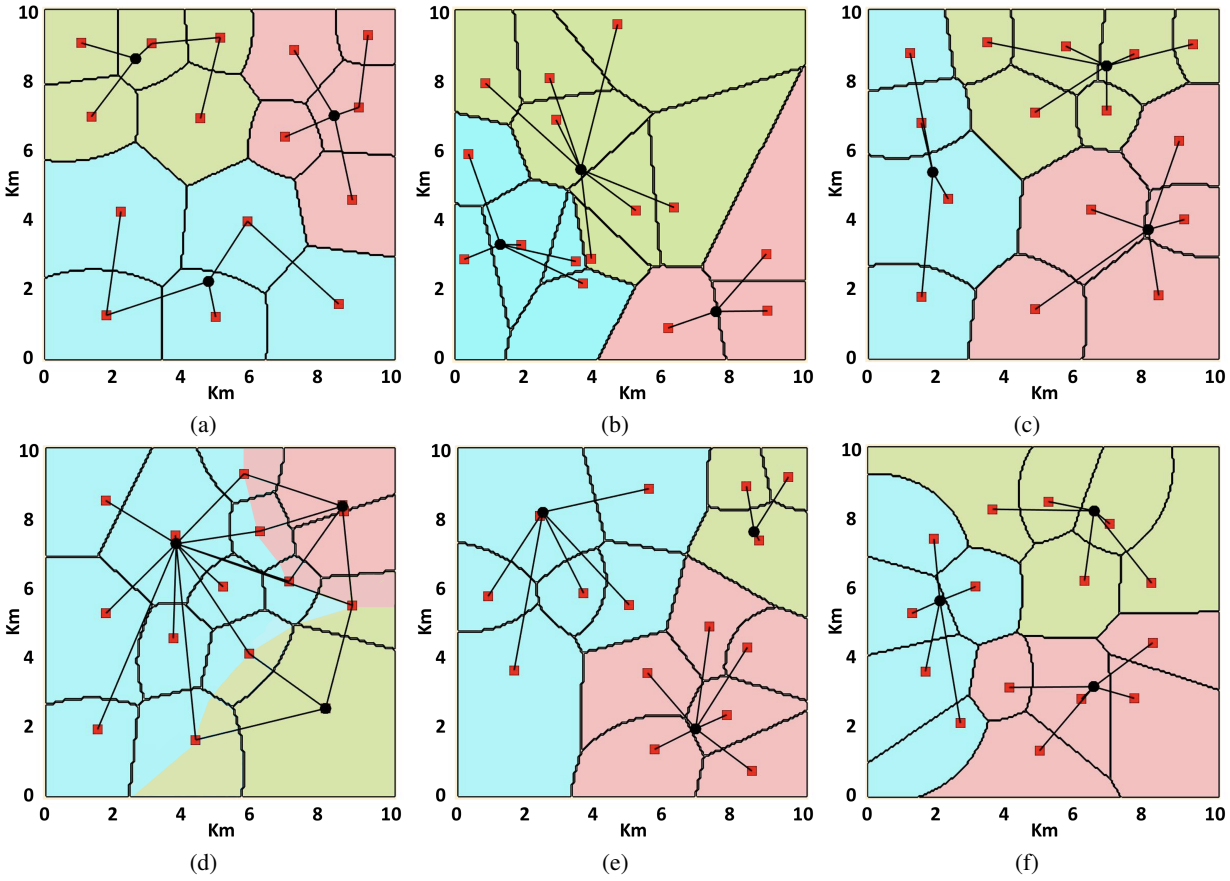

Fig. 3: Node deployment for Gaussian mixture PDF. (a) CF (b) GA (c) HTTL (d) POOL (e) PSO (f) VFA.

as it plays a vital role in achieving adequate signal strength and minimizing communication bottlenecks. In Figure 4, the POOL algorithm is executed on the same network configuration as before, with the exception of setting $\lambda = 1.0$ for which $\mathcal{P}(\mathbf{P}, \mathbf{Q}, \mathbf{W}, \mathbf{R})$ represents the total power consumption of the network. The algorithm is applied to a uniform distribution of sensors, but with varying numbers of APs. Figure 4 visually illustrates the relationship between the number of APs and the network's power consumption, offering a quantitative measure for selecting the appropriate number of APs to achieve specific performance objectives. For instance, based on Figure 4, it is observed that a minimum of 40 APs is required to ensure that the total power consumption of the network remains below 3.5W.

Next, we study the trade-off between sensors' and APs' power consumption that is parameterized by λ in Eq. (6). For small values of λ, sensor power consumption is the dominant component of $\mathcal{P}$; thus, it is more paramount to reduce the sensors' power consumption rather than APs' power consumption to minimize $\mathcal{P}$. However, increasing λ puts more weight on the

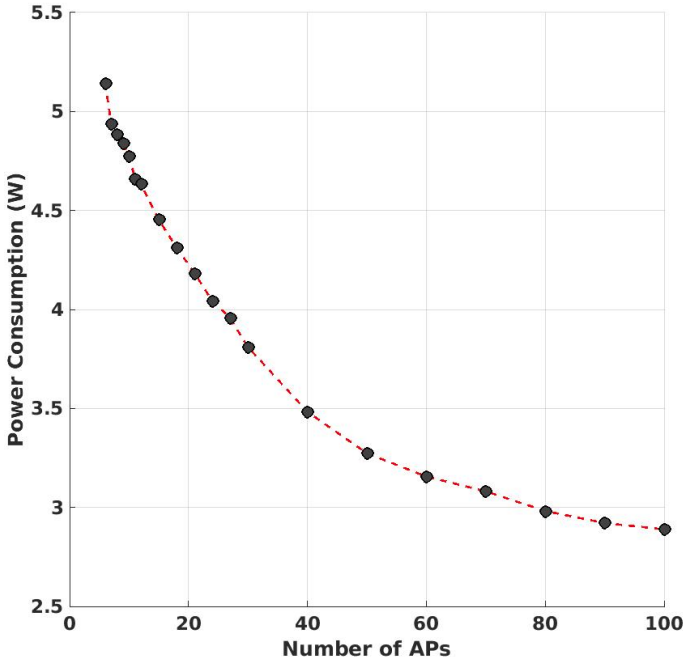

Fig. 4: The network power consumption as a function of the number of APs. Simulations for the POOL algorithm are carried out for the uniform distribution of sensors and $\lambda = 1$.

APs' power consumption. This effect is demonstrated in Fig. 5 where for the same initial node deployment, we increase the value of λ from 0 to 1. As expected, increasing λ reduces the APs' power consumption but increases the sensors' power consumption. Eq. (12) provides an alternative intuitive explanation for this observation because as λ increases, APs tend to be closer to BSs and farther away from centroids and sensors. As shown in Fig. 5, the Gaussian mixture requires less power compared to the uniform sensor distribution. This is because sensors are concentrated around the mean values of mixture components and can be covered with less average distances compared to the uniform distribution.

Finally, we illustrate how to systematically select the Lagrangian multiplier λ. There is a one-to-one correspondence between a point on the sensor-AP power curve in Fig. 5 and the value of λ. For example, the value of $\lambda = 0.4$ corresponds to the point on the Gaussian mixture curve in Fig. 5 with the sensor and AP power consumption of 404mW and 464mW, respectively. This means if there is a 404mW constraint on the sensor power, the minimum possible AP power consumption will be 464mW. Now, if a lower power constraint on the sensors is desirable, for example, 318mW, then a choice of smaller λ, i.e., $\lambda = 0.2$ results in a minimum possible AP power consumption of 733mW. The sensor-AP power curve in Fig. 5 contains enough information about

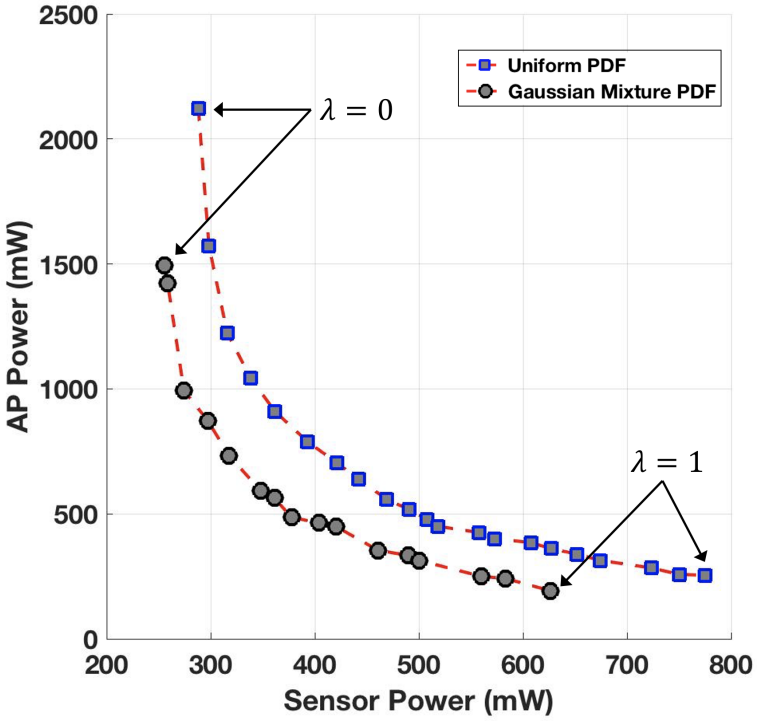

Fig. 5: AP-Sensor power trade-off in POOL Algorithm for both uniform and mixture of Gaussian PDFs. For the uniform PDF case, the blue square points represent the values of λ ranging from 0 to 1 in increments of 0.05, specifically: 0, 0.05, 0.1, 0.15, 0.2, 0.25, 0.3, 0.35, 0.4, 0.45, 0.5, 0.55, 0.6, 0.65, 0.7, 0.75, 0.8, 0.85, 0.9, 0.95, and 1. Similarly, for the mixture of Gaussian PDF case, the black circle points correspond to the values of λ ranging from 0 to 1, with the following specific values: 0, 0.05, 0.1, 0.15, 0.2, 0.25, 0.3, 0.35, 0.4, 0.45, 0.5, 0.55, 0.6, 0.65, 0.9, and 1.

the tradeoff between the optimal sensor and AP power consumption to select the appropriate λ value given an additional application specific constraint on the sensor or AP power.

V. Conclusion

A heterogeneous Rayleigh fading sensor network is presented and discussed in which a set of access points acts as relay nodes to facilitate the transfer of sensory data from sensors to base stations by the means of wireless communication. By considering both large-scale and small-scale propagation effects on the communication channels, our goal is to minimize the wireless transmission power consumption of the network subject to outage probability constraints on all wireless links. We derive the theoretical necessary conditions for the optimal deployment, cell partitioning, and data routing that minimizes the network's power consumption and accordingly devise an iterative algorithm to deploy nodes. Simulation results show that our proposed node deployment algorithm significantly reduces the communication power consumption in such networks and achieves superior performance compared to other techniques in the literature. It is

crucial to acknowledge that although the main emphasis of this manuscript has been on reducing the overall communication power consumption of the network, which can enhance the energy efficiency of the entire network, it does not automatically guarantee an optimal network lifetime. To achieve a specific network lifetime, it becomes necessary to modify the objective function accordingly, aiming for a more equitable power distribution among sensor nodes instead of solely minimizing the overall power consumption. This aspect represents an intriguing extension to our present research and is the subject of our future study.

APPENDIX A
PROOF OF PROPOSITION 1

For a fixed cell partitioning $\mathbf{W}$ and data routing $\mathbf{R}$, we can rewrite the objective function $\mathcal{P}$ in Eq. (11) using the parallel axis theorem [46] as follows:

$$\begin{aligned}\mathcal{P}(\mathbf{P},\mathbf{Q},\mathbf{W},\mathbf{R}) = &\sum_{n=1}^{N}\int_{W_n}\frac{a_n}{\ln\left(\frac{1}{1-\epsilon}\right)}\|c_n-\omega\|^2\Big(2^{\frac{R_b}{B}}-1\Big)f(\omega)d\omega\\ &+\sum_{n=1}^{N}\frac{a_n}{\ln\left(\frac{1}{1-\epsilon}\right)}\|p_n-c_n\|^2\Big(2^{\frac{R_b}{B}}-1\Big)v_n\\ &+\lambda\sum_{n=1}^{N}\sum_{m=1}^{M}\frac{b_{n,m}}{\ln\left(\frac{1}{1-\epsilon}\right)}\|p_n-q_m\|^2\Big(2^{\frac{F_{n,m}}{B}}-1\Big),\end{aligned} \tag{18}$$

where v_n and c_n are the volume and centroid of region W_n, respectively. Since the optimal deployment satisfies the zero gradient condition, we take the partial derivatives of Eq. (18) with respect to AP and BS locations as follows. For each $n \in \mathcal{I}_{AP}$, we have:

$$\frac{\partial\mathcal{P}}{\partial p_n^*} = \frac{2a_n}{\ln\left(\frac{1}{1-\epsilon}\right)}\big(p_n^*-c_n\big)\Big(2^{\frac{R_b}{B}}-1\Big)v_n+\lambda\sum_{m=1}^{M}\frac{2b_{n,m}}{\ln\left(\frac{1}{1-\epsilon}\right)}\big(p_n^*-q_m^*\big)\Big(2^{\frac{F_{n,m}}{B}}-1\Big)=0. \tag{19}$$

By solving Eq. (19), we directly obtain Eq. (12). Now, for each $m \in \mathcal{I}_{BS}$, we have:

$$\frac{\partial\mathcal{P}}{\partial q_m^*} = \lambda\sum_{n=1}^{N}\frac{2b_{n,m}}{\ln\left(\frac{1}{1-\epsilon}\right)}\big(q_m^*-p_n^*\big)\Big(2^{\frac{F_{n,m}}{B}}-1\Big)=0. \tag{20}$$

By solving Eq. (20), we obtain Eq. (13) and the proof is complete. ■

APPENDIX B
PROOF OF LEMMA 1

First, we prove the following lemma.

Lemma 2: For a constant $d \in \mathbb{R}$, the geometric locus of points $\omega \in \mathbb{R}^2$ that satisfy the equation

$$a_i\|p_i - \omega\|^2 - a_j\|p_j - \omega\|^2 = d, \tag{21}$$

is a line perpendicular to $\overline{p_ip_j}$ in case $a_i = a_j$, and either a circle centered at $c = \frac{a_ip_i - a_jp_j}{a_i - a_j}$ or an empty set in case $a_i \neq a_j$.

Proof: First, we consider the case where $a_i = a_j = a$. Let h be the projection of the point ω on the line $\overline{p_ip_j}$. Using Pythagoras' theorem, we can rewrite Eq. (21) as follows:

$$\left(\|p_i - h\|^2 + \|h - \omega\|^2\right) - \left(\|p_j - h\|^2 + \|h - \omega\|^2\right) = \left(\|p_i - h\|^2 - \|p_j - h\|^2\right) = \frac{d}{a}, \tag{22}$$

thus, any point ω whose projection on the line $\overline{p_ip_j}$ is h satisfies Eq. (21). Therefore, the geometric locus of the point ω is a line perpendicular to the line $\overline{p_ip_j}$. Now, we consider the case where $a_i \neq a_j$. Let $p = (p_x, p_y)$ and $\omega = (\omega_x, \omega_y)$. We can rewrite Eq. (21) as:

$$(a_i - a_j)\left(\omega_x^2 + \omega_y^2\right) - 2\left(a_ip_{ix} - a_jp_{jx}\right)\omega_x - 2\left(a_ip_{iy} - a_jp_{jy}\right)\omega_y = d - \left(a_i\|p_i\|^2 - a_j\|p_j\|^2\right) \tag{23}$$

or equivalently:

$$\left[\omega_x - \frac{a_ip_{ix} - a_jp_{jx}}{a_i - a_j}\right]^2 + \left[\omega_y - \frac{a_ip_{iy} - a_jp_{jy}}{a_i - a_j}\right]^2 = d', \tag{24}$$

where $d' = \frac{d - \left(a_i\|p_i\|^2 - a_j\|p_j\|^2\right)}{a_i - a_j} + \frac{(a_ip_{ix} - a_jp_{jx})^2 + (a_ip_{iy} - a_jp_{jy})^2}{(a_i - a_j)^2}$. Hence, the geometric locus of the point ω is either an empty set if $d' < 0$ or a circle centered at $c = \frac{a_ip_i - a_jp_j}{a_i - a_j}$ with radius $\kappa = \sqrt{d'}$ and Lemma 2 is proved. ■

Now, we use proof by contradiction to establish Lemma 1. Let v_i^* and v_j^* be the volume of the neighboring regions W_i^* and W_j^*, respectively, and assume that the optimal boundary $\delta_{i,j}^*$ is neither a segment if $a_i = a_j$, nor an arc in case $a_i \neq a_j$. Let $m_{i,j}(\alpha) = \alpha p_i + (1 - \alpha)p_j$, for $\alpha \in \mathbb{R}$, be a point on the line $\overline{p_ip_j}$ and define two regions W_i' and W_j' as:

$$W_i' = \left\{\omega \mid \omega \in \Omega_{i,j}^*, a_i\|p_i - \omega\|^2 - a_j\|p_j - \omega\|^2 \leq a_i\|p_i - m_{i,j}(\alpha)\|^2 - a_j\|p_j - m_{i,j}(\alpha)\|^2\right\}, \tag{25}$$

$$W_j' = \left\{\omega \mid \omega \in \Omega_{i,j}^*, a_i\|p_i - \omega\|^2 - a_j\|p_j - \omega\|^2 \geq a_i\|p_i - m_{i,j}(\alpha)\|^2 - a_j\|p_j - m_{i,j}(\alpha)\|^2\right\}, \tag{26}$$

where $\Omega_{i,j}^* = W_i^* \cup W_j^*$, and let $v_i'(\alpha)$ and $v_j'(\alpha)$ be the volume of regions W_i' and W_j', respectively. Note that since the sensor density function $f(\omega)$ is a continuous and differentiable function, both $v_i'(\alpha)$ and $v_j'(\alpha)$ are continuous functions of α. The geometric implications of Lemma 2 can be

understood as follows: the locus of points $\omega \in \mathbb{R}^2$ satisfying the equation $a_i\|p_i-\omega\|^2 - a_j\|p_j-\omega\|^2 = a_i\|p_i - m_{i,j}(\alpha)\|^2 - a_j\|p_j - m_{i,j}(\alpha)\|^2$ can be described differently depending on the values of a_i and a_j. When $a_i = a_j$, the locus forms a line perpendicular to $\overline{p_i p_j}$ at the point $m_{i,j}(\alpha)$, according to Lemma 2. On the other hand, when $a_i \neq a_j$, the locus becomes a circle centered at $c_{i,j} = \frac{a_i p_i - a_j p_j}{a_i - a_j}$ with a radius of $\kappa_{i,j}(\alpha) = \|c_{i,j} - m_{i,j}(\alpha)\|$. We can further deduce that for $a_i < a_j$, if α is sufficiently large, $v_i'(\alpha)$ becomes zero, and if $\alpha = \frac{a_i}{a_i - a_j}$, then $v_j'(\alpha)$ becomes zero, resulting in $\kappa_{i,j}(\alpha) = 0$. Likewise, for $a_i > a_j$, if $\alpha = \frac{a_i}{a_i - a_j}$, $\kappa_{i,j}(\alpha)$ and $v_i'(\alpha)$ becomes zero, and if α is sufficiently large, $v_j'(\alpha)$ becomes zero. Finally, when $a_i = a_j$, for large α values, $v_i'(\alpha)$ becomes zero, and for small α values, $v_j'(\alpha)$ becomes zero.

Using the above argument and the fact that $v_i'(\alpha) + v_j'(\alpha) = v_i^* + v_j^*$, it follows that there exists an α^* for which we have $v_i'(\alpha^*) = v_i^*$ and $v_j'(\alpha^*) = v_j^*$. Now, we define a new cell partitioning $\mathbf{W}'' = (W_1'', \cdots, W_N'')$ where $W_t'' = W_t^*$ for $t \notin \{i, j\}$, $W_i'' = W_i'(\alpha^*)$, and $W_j'' = W_j'(\alpha^*)$. Then, substituting $\mathbf{W}^*$ with $\mathbf{W}''$ will increase the objective function by:

$$\begin{aligned}
\Delta = &\left[\sum_{n=1}^{N}\int_{W_n''}\frac{a_n}{\ln\left(\frac{1}{1-\epsilon}\right)}\|p_n-\omega\|^2\left(2^{\frac{R_b}{B}}-1\right)f(\omega)d\omega\right.\\
&\left.+\lambda\sum_{i=1}^{N}\sum_{j=1}^{M}\frac{b_{i,j}}{\ln\left(\frac{1}{1-\epsilon}\right)}\|p_i-q_j\|^2\left(2^{\frac{r_{i,j}\times R_b\times v_i''}{B}}-1\right)\right]\\
&-\left[\sum_{n=1}^{N}\int_{W_n^*}\frac{a_n}{\ln\left(\frac{1}{1-\epsilon}\right)}\|p_n-\omega\|^2\left(2^{\frac{R_b}{B}}-1\right)f(\omega)d\omega\right.\\
&\left.+\lambda\sum_{i=1}^{N}\sum_{j=1}^{M}\frac{b_{i,j}}{\ln\left(\frac{1}{1-\epsilon}\right)}\|p_i-q_j\|^2\left(2^{\frac{r_{i,j}\times R_b\times v_i^*}{B}}-1\right)\right].
\end{aligned} \tag{27}$$

Note that $W_t'' = W_t^*$ for $t \notin \{i, j\}$ and $v_t'' = v_t^*$ for all $t \in \{1, \cdots, N\}$. Hence, we have:

$$\begin{aligned}
\frac{\Delta \times \ln\left(\frac{1}{1-\epsilon}\right)}{\left(2^{\frac{R_b}{B}}-1\right)} = &\left[\int_{W_i''}a_i\|p_i-\omega\|^2 f(\omega)d\omega + \int_{W_j''}a_j\|p_j-\omega\|^2 f(\omega)d\omega\right]\\
&-\left[\int_{W_i^*}a_i\|p_i-\omega\|^2 f(\omega)d\omega + \int_{W_j^*}a_j\|p_j-\omega\|^2 f(\omega)d\omega\right].
\end{aligned} \tag{28}$$

Let $\mathcal{V}_1 = W_i'' \cap W_j^*$ and $\mathcal{V}_2 = W_j'' \cap W_i^*$. Note that both $\mathcal{V}_1$ and $\mathcal{V}_2$ are non-empty; otherwise, we have $W_i'' = W_i^*$ and $W_j'' = W_j^*$ which contradicts the assumption that the optimal boundary

$\delta^*_{i,j}$ is not a segment or an arc. Now, we can rewrite Eq. (28) as follows:

$$\begin{aligned}
\frac{\Delta \times \ln\left(\frac{1}{1-\epsilon}\right)}{\left(2^{\frac{R_b}{B}}-1\right)} &= \left[\int_{\mathcal{V}_1} a_i\|p_i-\omega\|^2 f(\omega)d\omega + \int_{\mathcal{V}_2} a_j\|p_j-\omega\|^2 f(\omega)d\omega\right] \\
&\quad - \left[\int_{\mathcal{V}_2} a_i\|p_i-\omega\|^2 f(\omega)d\omega + \int_{\mathcal{V}_1} a_j\|p_j-\omega\|^2 f(\omega)d\omega\right] \qquad (29)\\
&= \int_{\mathcal{V}_1} \left(a_i\|p_i-\omega\|^2 - a_j\|p_j-\omega\|^2\right) f(\omega)d\omega \\
&\quad + \int_{\mathcal{V}_2} \left(a_j\|p_j-\omega\|^2 - a_i\|p_i-\omega\|^2\right) f(\omega)d\omega \qquad (30)\\
&< \int_{\mathcal{V}_1} \left(a_i\left\|p_i-m_{i,j}(\alpha^*)\right\|^2 - a_j\left\|p_j-m_{i,j}(\alpha^*)\right\|^2\right) f(\omega)d\omega \\
&\quad + \int_{\mathcal{V}_2} \left(a_j\left\|p_j-m_{i,j}(\alpha^*)\right\|^2 - a_i\left\|p_i-m_{i,j}(\alpha^*)\right\|^2\right) f(\omega)d\omega \qquad (31)\\
&= \left(a_i\left\|p_i-m_{i,j}(\alpha^*)\right\|^2 - a_j\left\|p_j-m_{i,j}(\alpha^*)\right\|^2\right)\times\left(\int_{\mathcal{V}_1} f(\omega)d\omega - \int_{\mathcal{V}_2} f(\omega)d\omega\right) \qquad (32)\\
&= 0, \qquad (33)
\end{aligned}$$

where the inequality in (31) follows from Lemma 2 and the fact that both $\mathcal{V}_1$ and $\mathcal{V}_2$ are non-empty. Also, Eq. (33) follows from the fact that $\mathcal{V}_1$ and $\mathcal{V}_2$ have the same volume because $v''_i = v^*_i$ and $v''_j = v^*_j$. Since $0 < \epsilon < 1$ and $R_b > 0$, it follows from Eqs. (29)−(33) that

$$\frac{\Delta \times \ln\left(\frac{1}{1-\epsilon}\right)}{\left(2^{\frac{R_b}{B}}-1\right)} < 0 \qquad \Longrightarrow \qquad \Delta < 0, \qquad (34)$$

i.e., the increase in the objective function is negative. Thus, $\mathbf{W}''$ yields a lower objective function than that of $\mathbf{W}^*$ which contradicts the optimality of $\mathbf{W}^*$ and the proof is complete. ■

APPENDIX C
PROOF OF PROPOSITION 2

According to Lemma 1, the optimal boundary $\delta^*_{i,j}$, which intersects the line $\overline{p_ip_j}$ at $h^*_{i,j}$, is either a segment if $a_i = a_j$, or an arc with its center placed at $c = \frac{a_ip_i - a_jp_j}{a_i - a_j}$ if $a_i \neq a_j$. Let α^* be the scalar that satisfies the equation $\alpha^* p_i + (1-\alpha^*)p_j = h^*_{i,j}$. For an infinitesimal $\gamma > 0$, let $\alpha' = \alpha^* - \gamma$. Then, we define a new cell partitioning $\mathbf{W}' = \left(W'_1, \cdots, W'_N\right)$ as follows:

$$W'_i = \left\{\omega \mid \omega \in \Omega^*_{i,j}, a_i\|p_i-\omega\|^2 - a_j\|p_j-\omega\|^2 \leq a_i\|p_i-h'_{i,j}\|^2 - a_j\|p_j-h'_{i,j}\|^2\right\}, \qquad (35)$$

$$W'_j = \big\{\omega \mid \omega \in \Omega^*_{i,j}, a_i\|p_i-\omega\|^2 - a_j\|p_j-\omega\|^2 \geq a_i\|p_i-h'_{i,j}\|^2 - a_j\|p_j-h'_{i,j}\|^2\big\}, \quad (36)$$

and $W'_t = W^*_t$ for $t \notin \{i,j\}$, where $\Omega^*_{i,j} = W^*_i \cup W^*_j$ and $h'_{i,j} = \alpha' p_i + (1-\alpha')p_j$. Note that the infinitesimal difference between α^* and α' leads to an infinitesimal difference between volumes of these new regions, i.e., $v'_i = v^*_i + dv$ and $v'_j = v^*_j - dv$, where v'_i and v'_j are the volumes of W'_i and W'_j, respectively, and dv is the volume of the region $dW = W'_i - W^*_i = W^*_j - W'_j$. By substituting $\mathbf{W}^*$ with $\mathbf{W}'$, the increase in the sensor power consumption can be written as:

$$\begin{aligned}\Delta_1 =& \int_{W'_i} \frac{a_i}{\ln\left(\frac{1}{1-\epsilon}\right)}\|p_i-\omega\|^2\Big(2^{\frac{R_b}{B}}-1\Big)f(\omega)d\omega + \int_{W'_j} \frac{a_j}{\ln\left(\frac{1}{1-\epsilon}\right)}\|p_j-\omega\|^2\Big(2^{\frac{R_b}{B}}-1\Big)f(\omega)d\omega \\ &- \int_{W^*_i} \frac{a_i}{\ln\left(\frac{1}{1-\epsilon}\right)}\|p_i-\omega\|^2\Big(2^{\frac{R_b}{B}}-1\Big)f(\omega)d\omega - \int_{W^*_j} \frac{a_j}{\ln\left(\frac{1}{1-\epsilon}\right)}\|p_j-\omega\|^2\Big(2^{\frac{R_b}{B}}-1\Big)f(\omega)d\omega \quad (37)\end{aligned}$$

which can be simplified as follows:

$$\begin{aligned}\Delta_1 =& \int_{dW} \frac{a_i}{\ln\left(\frac{1}{1-\epsilon}\right)}\|p_i-\omega\|^2\Big(2^{\frac{R_b}{B}}-1\Big)f(\omega)d\omega - \int_{dW} \frac{a_j}{\ln\left(\frac{1}{1-\epsilon}\right)}\|p_j-\omega\|^2\Big(2^{\frac{R_b}{B}}-1\Big)f(\omega)d\omega \quad (38)\\ =& \int_{dW} \frac{1}{\ln\left(\frac{1}{1-\epsilon}\right)}\Big[a_i\|p_i-\omega\|^2 - a_j\|p_j-\omega\|^2\Big]\Big(2^{\frac{R_b}{B}}-1\Big)f(\omega)d\omega. \quad (39)\end{aligned}$$

It follows from Lemma 2 and the definition of W'_i and W'_j in Eqs. (35) and (36) that for an infinitesimal region dW, we have:

$$\begin{aligned}\Delta_1 =& \int_{dW} \frac{1}{\ln\left(\frac{1}{1-\epsilon}\right)}\Big[a_i\|p_i-h^*_{i,j}\|^2 - a_j\|p_j-h^*_{i,j}\|^2\Big]\Big(2^{\frac{R_b}{B}}-1\Big)f(\omega)d\omega + \mathcal{O}(dv^2) \quad (40)\\ =& \frac{1}{\ln\left(\frac{1}{1-\epsilon}\right)}\Big[a_i\|p_i-h^*_{i,j}\|^2 - a_j\|p_j-h^*_{i,j}\|^2\Big]\Big(2^{\frac{R_b}{B}}-1\Big)dv + \mathcal{O}(dv^2). \quad (41)\end{aligned}$$

Now, substituting $\mathbf{W}^*$ with $\mathbf{W}'$ results in the following increase in the AP power consumption:

$$\begin{aligned}\Delta_2 =& \sum_{t=1}^{M} \frac{b_{i,t}}{\ln\left(\frac{1}{1-\epsilon}\right)}\|p_i-q_t\|^2\Big(2^{\frac{r_{i,t}R_b v'_i}{B}}-1\Big) + \sum_{t=1}^{M} \frac{b_{j,t}}{\ln\left(\frac{1}{1-\epsilon}\right)}\|p_j-q_t\|^2\Big(2^{\frac{r_{j,t}R_b v'_j}{B}}-1\Big)\\ &- \sum_{t=1}^{M} \frac{b_{i,t}}{\ln\left(\frac{1}{1-\epsilon}\right)}\|p_i-q_t\|^2\Big(2^{\frac{r_{i,t}R_b v^*_i}{B}}-1\Big) - \sum_{t=1}^{M} \frac{b_{j,t}}{\ln\left(\frac{1}{1-\epsilon}\right)}\|p_j-q_t\|^2\Big(2^{\frac{r_{j,t}R_b v^*_j}{B}}-1\Big) \quad (42)\\ =& \sum_{t=1}^{M} \frac{b_{i,t}}{\ln\left(\frac{1}{1-\epsilon}\right)}\|p_i-q_t\|^2 \times 2^{\frac{r_{i,t}R_b v^*_i}{B}} \times \Big(2^{\frac{r_{i,t}R_b dv}{B}}-1\Big)\\ &+ \sum_{t=1}^{M} \frac{b_{j,t}}{\ln\left(\frac{1}{1-\epsilon}\right)}\|p_j-q_t\|^2 \times 2^{\frac{r_{j,t}R_b v^*_j}{B}} \times \Big(2^{\frac{-r_{j,t}R_b dv}{B}}-1\Big), \quad (43)\end{aligned}$$

where Eq. (43) follows from the relations $v'_i = v^*_i + dv$ and $v'_j = v^*_j - dv$. Using the Taylor series expansion, we can write Eq. (43) as follows:

$$\Delta_2 = \sum_{t=1}^{M} \frac{b_{i,t}}{\ln\left(\frac{1}{1-\epsilon}\right)} \|p_i - q_t\|^2 \times 2^{\frac{r_{i,t}R_b v^*_i}{B}} \times \ln(2) \times \frac{r_{i,t}R_b dv}{B} - \sum_{t=1}^{M} \frac{b_{j,t}}{\ln\left(\frac{1}{1-\epsilon}\right)} \|p_j - q_t\|^2 \times 2^{\frac{r_{j,t}R_b v^*_j}{B}} \times \ln(2) \times \frac{r_{j,t}R_b dv}{B} + \mathcal{O}(dv^2), \tag{44}$$

where $\mathcal{O}(dv^2)$ contains terms of second and higher orders in the Taylor series approximation. By combining Eqs. (41) and (44), the total increase in the objective function due to substituting $\mathbf{W}^*$ with $\mathbf{W}'$ is given by $\Delta = \Delta_1 + \lambda\Delta_2$, that is:

$$\Delta = \frac{1}{\ln\left(\frac{1}{1-\epsilon}\right)} \left[a_i \|p_i - h^*_{i,j}\|^2 - a_j \|p_j - h^*_{i,j}\|^2\right] \left(2^{\frac{R_b}{B}} - 1\right) dv + \lambda \sum_{t=1}^{M} \frac{b_{i,t}}{\ln\left(\frac{1}{1-\epsilon}\right)} \|p_i - q_t\|^2 \times 2^{\frac{r_{i,t}R_b v^*_i}{B}} \times \ln(2) \times \frac{r_{i,t}R_b dv}{B} - \lambda \sum_{t=1}^{M} \frac{b_{j,t}}{\ln\left(\frac{1}{1-\epsilon}\right)} \|p_j - q_t\|^2 \times 2^{\frac{r_{j,t}R_b v^*_j}{B}} \times \ln(2) \times \frac{r_{j,t}R_b dv}{B} + \mathcal{O}(dv^2) \geq 0, \tag{45}$$

where the last inequality follows from the optimality of $\mathbf{W}^*$. By dividing Δ by dv and taking the limit $dv \longrightarrow 0$, the term $\mathcal{O}(dv^2)$ vanishes and we have:

$$\left[a_i \|p_i - h^*_{i,j}\|^2 - a_j \|p_j - h^*_{i,j}\|^2\right] \left(2^{\frac{R_b}{B}} - 1\right) + \lambda \sum_{t=1}^{M} b_{i,t} \|p_i - q_t\|^2 \times 2^{\frac{r_{i,t}R_b v^*_i}{B}} \times \ln(2) \times \frac{r_{i,t}R_b}{B} - \lambda \sum_{t=1}^{M} b_{j,t} \|p_j - q_t\|^2 \times 2^{\frac{r_{j,t}R_b v^*_j}{B}} \times \ln(2) \times \frac{r_{j,t}R_b}{B} \geq 0. \tag{46}$$

By defining $\alpha'' = \alpha^* + \gamma$ for an infinitesimal $\gamma > 0$ and repeating the same procedure, we obtain:

$$\left[a_i \|p_i - h^*_{i,j}\|^2 - a_j \|p_j - h^*_{i,j}\|^2\right] \left(2^{\frac{R_b}{B}} - 1\right) + \lambda \sum_{t=1}^{M} b_{i,t} \|p_i - q_t\|^2 \times 2^{\frac{r_{i,t}R_b v^*_i}{B}} \times \ln(2) \times \frac{r_{i,t}R_b}{B} - \lambda \sum_{t=1}^{M} b_{j,t} \|p_j - q_t\|^2 \times 2^{\frac{r_{j,t}R_b v^*_j}{B}} \times \ln(2) \times \frac{r_{j,t}R_b}{B} \leq 0. \tag{47}$$

By combining Eqs. (46) and (47), we obtain Eq. (14) and the proof is complete. ■

APPENDIX D
PROOF OF PROPOSITION 3

First, we prove the following lemma.

Lemma 3: Let $g(x) = a^x + a^{C-x}$ where $x \in [0, C]$ for $a, C \in \mathbb{R}^+$ and $a > 1$. Then, $g(.)$ is symmetric around the point $x = \frac{C}{2}$ and strictly decreasing in the interval $\left[0, \frac{C}{2}\right)$.

Proof: Function $g(.)$ is symmetric because $g(x) = g(C - x)$. Now, by taking the derivative w.r.t. x, we have $\frac{d}{dx}g(x) = \ln(a) \times \left(a^x - a^{C-x}\right)$. Since $a > 1$, we have $\frac{d}{dx}g(x) < 0$ for $x \in \left[0, \frac{C}{2}\right)$ and the proof is complete. ■

Lemma 3 leads to the following conclusion.

Corollary 1: Let x_1 and x_2 be two non-negative real numbers such that $x_1 + x_2 = C$ is a constant. Then, for $a > 1$, decreasing $|x_1 - x_2|$ results in smaller $a^{x_1} + a^{x_2}$ values.

Now, we proceed to establish Proposition 3. Note that the constrained objective function formulation in Eqs. (15)−(16) is equivalent to

$$\underset{F_{n,1},\cdots,F_{n,M}}{\arg\min} \sum_{i=1}^{M} 2^{\left[\frac{F_{n,i}}{B} + \log_2\left(b_{n,i}\|p_n - q_i\|^2\right)\right]}, \tag{48}$$

$$\text{s.t. } \sum_{i=1}^{M} F_{n,i} = \int_{W_n} R_b f(\omega) d\omega = R_b v_n, \quad \text{and} \quad F_{n,i} \geq 0 \text{ for all } i \in \mathcal{I}_{BS}, \tag{49}$$

which is equivalent to the following constrained objective function formulation:

$$\underset{x_{n,1},\cdots,x_{n,M}}{\arg\min} \sum_{i=1}^{M} 2^{x_{n,i}}, \tag{50}$$

$$\text{s.t. } \sum_{i=1}^{M} x_{n,i} = \frac{R_b v_n}{B} + \sum_{i=1}^{M} \log_2\left(b_{n,i}\|p_n - q_i\|^2\right) = C, \tag{51}$$

$$x_{n,i} \geq \log_2\left(b_{n,i}\|p_n - q_i\|^2\right) \text{ for all } i \in \{1, \cdots, M\}, \tag{52}$$

where $x_{n,i} = \frac{F_{n,i}}{B} + \log_2\left(b_{n,i}\|p_n - q_i\|^2\right)$. Corollary 1 indicates that for any two indices i and j, we can decrease the objective function in Eq. (50) by decreasing $|x_{n,i} - x_{n,j}|$ while keeping their summation constant. Thus, the minimum occurs when we have $x_{n,1} = \cdots = x_{n,M} = \frac{C}{M}$. However, this may contradict the constraint in Eq. (52) for some indices $i \in \{1, \cdots, M\}$. Therefore, we can always improve the objective function in Eq. (50) and achieve a lower value by decreasing the distance between any pair of $x_{n,i}$ and $x_{n,j}$ while keeping their summation constant as long as the constraints in Eq. (52) is not contradicted. This observation results in

Corollary 2: Let $X_n^* = (x_{n,1}^*, \cdots, x_{n,M}^*)$ be the optimal solution to the constrained objective function in Eqs. (50)−(52). Then, there exist unique sets I_L^* and I_U^* such that

$$x_{n,i}^* = x_{n,j}^* = \overline{x}^* \quad \text{for} \quad \forall i,j \in I_U^*, \qquad \text{and} \qquad x_{n,i}^* = \log_2\left(b_{n,i}\|p_n - q_i\|^2\right) \quad \text{for} \quad \forall i \in I_L^*, \tag{53}$$

and $x_{n,i}^* > \overline{x}^*$ for all $i \in I_L^*$.

To see why the last property holds, first, let us assume that we have $x_{n,j}^* = \log_2\left(b_{n,j}\|p_n - q_j\|^2\right)$ for all $j \in I_U^*$. Since $v_n > 0$, it follows that

$$\sum_{t=1}^{M} x_{n,t}^* = \sum_{t\in I_U^*} x_{n,t}^* + \sum_{t\in I_L^*} x_{n,t}^* = \sum_{t=1}^{M} \log_2\left(b_{n,t}\|p_n - q_t\|^2\right) < C, \tag{54}$$

which is in contradiction with Eq. (51). Hence, there exists an index $j' \in I_U^*$ for which $x_{n,j'}^* > \log_2\left(b_{n,j'}\|p_n - q_{j'}\|^2\right)$. Now, assume that there exists an index i such that $x_{n,i}^* = \log_2\left(b_{n,i}\|p_n - q_i\|^2\right) < \overline{x}^* = x_{n,j'}^*$. Then, according to Corollary 1, we can achieve a lower objective function by replacing $x_{n,i}^*$ and $x_{n,j'}^*$ with $x_{n,i}^* + \eta$ and $x_{n,j'}^* - \eta$ for any $0 < \eta < x_{n,j'}^* - \log_2\left(b_{n,j'}\|p_n - q_{j'}\|^2\right)$, which contradicts the optimality of X_n^*. Thus, we have $x_{n,i}^* > \overline{x}^*$ for all $i \in I_L^*$.

Corollary 2 indicates that in an optimal solution, all $x_{n,t}^*$ values should be equal to some value $\overline{x}^*$ except for those that cannot get close enough to $\overline{x}^*$ without contradicting Eq. (52). Hence, the optimal solution can be found using a water filling algorithm as follows. By initializing I_L to an empty set and starting from the case in which all $x_{n,t}$ values are equal to the mean value $\overline{x} = \frac{C}{M}$, we can identify those indices such as $i \in I$ for which $x_{n,i} < \log_2\left(b_{n,i}\|p_n - q_i\|^2\right)$. Thus, I provides the first series of indices for which the value of $x_{n,i}$ cannot be reduced enough to the mean value $\overline{x}$ without contradicting the constraint in Eq. (52). Therefore, the optimal value for each $i \in I$ is $x_{n,i}^* = \log_2\left(b_{n,i}\|p_n - q_i\|^2\right)$ and we update the set I_L by taking its union with the set I. Now, we can update the mean value $\overline{x}$ such that $\sum_{i\in\mathcal{I}_{BS}\setminus I_L} \overline{x} + \sum_{i\in I_L} x_{n,i}^*$ or equivalently $\left(M - |I_L|\right) \times \overline{x} + \sum_{i\in I_L} \log_2\left(b_{n,i}\|p_n - q_i\|^2\right)$ still sums to C. By using the new mean value $\overline{x}$, we can determine the next series of indices that would belong to I_L and the same procedure can be repeated. Note that in each iteration, the mean value $\overline{x}$ either decreases or stays the same and the set I_L either increases in size or stays the same. If I_L stays the same, meaning that there has been no other index that would contradict Eq. (52), then we have found the optimal solution and the algorithm terminates. Since $|I_L| \leq M$, the process of I_L increasing in size can continue for at most M iterations and the algorithm will finally converge to the optimal value X_n^* that satisfies Eq. (53) in Corollary 2. The above procedure is summarized in

Algorithm 1. Note that the optimal values $F^*_{n,1}, \cdots, F^*_{n,M}$ in Eqs. (48) and (49) can then be found as $F^*_{n,i} = B \times \left[x^*_{n,i} - \log_2\left(b_{n,i}\|p_n - q_i\|^2\right)\right]$ and the proof is complete. ■

APPENDIX E
PROOF OF PROPOSITION 4

First, we aim to prove the convergence of the initialization step that is outlined in Algorithm 2. Note that the generalized Voronoi diagram $\mathcal{V}$ in Algorithm 2 provides the optimal cell partitioning for the following cost function:

$$\mathcal{D}'(\mathbf{P}, \mathbf{W}) = \sum_{n=1}^{N} \int_{W_n} a_n \|p_n - \omega\|^2 f(\omega) d\omega. \tag{55}$$

Thus, for a fixed AP deployment $\mathbf{P}$, updating $\mathbf{W}$ according to $\mathcal{V}$ does not increase the cost function $\mathcal{D}'$. Now, using the parallel axis theorem, we can rewrite Eq. (55) as follows:

$$\mathcal{D}'(\mathbf{P}, \mathbf{W}) = \sum_{n=1}^{N} \int_{W_n} a_n \|p_n - c_n\|^2 f(\omega) d\omega + \sum_{n=1}^{N} \int_{W_n} a_n \|c_n - \omega\|^2 f(\omega) d\omega. \tag{56}$$

Hence, for a fixed cell partitioning $\mathbf{W}$, updating $\mathbf{P}$ according to the rule $p_n = c_n = \frac{\int_{W_n} \omega f(\omega) d\omega}{\int_{W_n} f(\omega) d\omega}$ does not increase the cost function $\mathcal{D}'$ in Eq. (56) either. Therefore, by iterating this process, a sequence of non-increasing $\mathcal{D}'$ values are generated and since $\mathcal{D}' \geq 0$, it will converge.

Note that base stations are initialized by applying the Lloyd algorithm to the set of AP points, which is known to converge. Finally, the normalized flow matrix $\mathbf{R}$ is updated by applying Algorithm 1, which we showed to converge in Appendix D. Thus, the initialization step which is outlined in Algorithm 2 will eventually converge.

To establish the convergence of the POOL algorithm, we show that none of the three steps corresponding to updating the node deployment, cell partitioning, and normalized flow matrix will increase the objective function $\mathcal{P}$. Note that when $\mathbf{W}$, $\mathbf{R}$, $\mathbf{Q}$, and $\{p_j\}_{j \neq i}$ are fixed, the objective function $\mathcal{P}$ is a convex function of p_i; thus, updating p_i according to Eq. (12), which is the solution to the zero-gradient equation, does not increase the objective function. Similarly, once $\mathbf{W}$, $\mathbf{R}$, $\mathbf{P}$, and $\{q_j\}_{j \neq i}$ are fixed, $\mathcal{P}$ is a convex function of q_i. Therefore, updating q_i according to Eq. (13), which is the solution to the zero-gradient equation, does not increase $\mathcal{P}$. Hence, the node deployment step of the POOL algorithm does not increase the objective function. Note that the cell partitioning is updated through an iterative process where at each step, two neighboring regions such as W_i and W_j are selected and their boundary is adjusted.

More precisely, in each iteration, all W_t regions for $t \notin \{i, j\}$ are held fixed and only the boundary $\delta_{i,j}$ between regions W_i and W_j is adjusted to provide another partitioning of the region $\Omega_{i,j} = W_i \cup W_j$. According to Proposition 2, this new partitioning is optimal; hence, the objective function $\mathcal{P}$ will not increase as a result of updating $\delta_{i,j}$. Finally, Proposition 3 indicates that updating the normalized flow matrix according to Algorithm 1 yields the optimal value of $\mathbf{R}$ and as such, $\mathcal{P}$ will either remain the same or decrease. Therefore, Algorithm 2 generates a non-increasing sequence of $\mathcal{P}$ values in each iteration, i.e., the POOL algorithm is an iterative improvement algorithm and since $\mathcal{P} \geq 0$, it will converge. ■

REFERENCES

[1] Y.-J. Chang, C.-H. Chen, L.-F. Lin, R.-P. Han, W.-T. Huang, and G.-C. Lee, "Wireless sensor networks for vital signs monitoring: Application in a nursing home," *International Journal of Distributed Sensor Networks*, vol. 8, no. 11, p. 685107, 2012.

[2] E. Felemban, "Advanced border intrusion detection and surveillance using wireless sensor network technology," *International Journal of Communications, Network and System Sciences*, vol. 6, no. 5, pp. 251–259, 2013.

[3] A. Z. Abbasi, N. Islam, Z. A. Shaikh, *et al.*, "A review of wireless sensors and networks' applications in agriculture," *Computer Standards & Interfaces*, vol. 36, no. 2, pp. 263–270, 2014.

[4] J. Aponte-Luis, J. A. Gómez-Galán, F. Gómez-Bravo, M. Sánchez-Raya, J. Alcina-Espigado, and P. M. Teixido-Rovira, "An efficient wireless sensor network for industrial monitoring and control," *Sensors*, vol. 18, no. 1, p. 182, 2018.

[5] J. Yick, B. Mukherjee, and D. Ghosal, "Wireless sensor network survey," *Computer networks*, vol. 52, no. 12, pp. 2292–2330, 2008.

[6] J. Zheng and A. Jamalipour, *Wireless sensor networks: a networking perspective*. John Wiley & Sons, 2009.

[7] P. Jiang, "A new method for node fault detection in wireless sensor networks," *Sensors*, vol. 9, no. 02, pp. 1282–1294, 2009.

[8] M. Farsi, M. A. Elhosseini, M. Badawy, H. A. Ali, and H. Z. Eldin, "Deployment techniques in wireless sensor networks, coverage and connectivity: A survey," *Ieee Access*, vol. 7, pp. 28940–28954, 2019.

[9] M. A. Matin and M. Islam, "Overview of wireless sensor network," *Wireless sensor networks-technology and protocols*, vol. 1, no. 3, 2012.

[10] H. Yousefi'zadeh, H. Jafarkhani, and M. Moshfeghi, "Power optimization of wireless media systems with space-time block codes," *IEEE Transactions on Image Processing*, vol. 13, pp. 873–884, Jun 2004.

[11] W. Liu, X. Zhou, S. Durrani, H. Mehrpouyan, and S. D. Blostein, "Energy harvesting wireless sensor networks: Delay analysis considering energy costs of sensing and transmission," *IEEE Transactions on Wireless Communications*, vol. 15, no. 7, pp. 4635–4650, 2016.

[12] Z. Sheng, C. Mahapatra, V. C. Leung, M. Chen, and P. K. Sahu, "Energy efficient cooperative computing in mobile wireless sensor networks," *IEEE Transactions on Cloud Computing*, vol. 6, no. 1, pp. 114–126, 2015.

[13] M. M. Warrier and A. Kumar, "Energy efficient routing in wireless sensor networks: A survey," in *2016 International Conference on Wireless Communications, Signal Processing and Networking (WiSPNET)*, pp. 1987–1992, IEEE, 2016.

[14] R. Wan, N. Xiong, *et al.*, "An energy-efficient sleep scheduling mechanism with similarity measure for wireless sensor networks," *Human-centric Computing and Information Sciences*, vol. 8, no. 1, pp. 1–22, 2018.

[15] S. Radhika and P. Rangarajan, "Fuzzy based sleep scheduling algorithm with machine learning techniques to enhance energy efficiency in wireless sensor networks," *Wireless Personal Communications*, vol. 118, no. 4, pp. 3025–3044, 2021.

[16] M. N. Khan, H. U. Rahman, M. A. Almaiah, M. Z. Khan, A. Khan, M. Raza, M. Al-Zahrani, O. Almomani, and R. Khan, "Improving energy efficiency with content-based adaptive and dynamic scheduling in wireless sensor networks," *IEEE Access*, vol. 8, pp. 176495–176520, 2020.

[17] J. K. Pabani, M.-Á. Luque-Nieto, W. Hyder, and A. Ariza, "Energy-efficient routing protocol for selecting relay nodes in underwater sensor networks based on fuzzy analytical hierarchy process," *Sensors*, vol. 22, no. 22, p. 8930, 2022.

[18] S. Saranya and M. Princy, "Routing techniques in sensor network–a survey," *Procedia engineering*, vol. 38, pp. 2739–2747, 2012.

[19] M. Benaddy, B. El Habil, M. El Ouali, O. El Meslouhi, and S. Krit, "A mutlipath routing algorithm for wireless sensor networks under distance and energy consumption constraints for reliable data transmission," in *2017 International Conference on Engineering & MIS (ICEMIS)*, pp. 1–4, IEEE, 2017.

[20] C. Nakas, D. Kandris, and G. Visvardis, "Energy efficient routing in wireless sensor networks: A comprehensive survey," *Algorithms*, vol. 13, no. 3, p. 72, 2020.

[21] Z. A. Eu and H.-P. Tan, "Adaptive opportunistic routing protocol for energy harvesting wireless sensor networks," in *2012 IEEE international conference on communications (ICC)*, pp. 318–322, IEEE, 2012.

[22] H. Mostafaei, "Energy-efficient algorithm for reliable routing of wireless sensor networks," *IEEE Transactions on Industrial Electronics*, vol. 66, no. 7, pp. 5567–5575, 2018.

[23] M. Sajwan, D. Gosain, and A. K. Sharma, "Hybrid energy-efficient multi-path routing for wireless sensor networks," *Computers & Electrical Engineering*, vol. 67, pp. 96–113, 2018.

[24] M. Abo-Zahhad, N. Sabor, S. Sasaki, and S. M. Ahmed, "A centralized immune-voronoi deployment algorithm for coverage maximization and energy conservation in mobile wireless sensor networks," *Information Fusion*, vol. 30, pp. 36–51, 2016.

[25] P. Chatterjee, S. C. Ghosh, and N. Das, "Load balanced coverage with graded node deployment in wireless sensor networks," *IEEE Transactions on Multi-Scale Computing Systems*, vol. 3, no. 2, pp. 100–112, 2017.

[26] M. S. Aliyu, A. H. Abdullah, H. Chizari, T. Sabbah, and A. Altameem, "Coverage enhancement algorithms for distributed mobile sensors deployment in wireless sensor networks," *International Journal of Distributed Sensor Networks*, vol. 12, no. 3, p. 9169236, 2016.

[27] S. Karimi-Bidhendi, J. Guo, and H. Jafarkhani, "Energy-efficient node deployment in heterogeneous two-tier wireless sensor networks with limited communication range," *IEEE Transactions on Wireless Communications*, vol. 20, no. 1, pp. 40–55, 2020.

[28] S. Karimi-Bidhendi, J. Guo, and H. Jafarkhani, "Using quantization to deploy heterogeneous nodes in two-tier wireless sensor networks," in *2019 IEEE International Symposium on Information Theory (ISIT)*, pp. 1502–1506, IEEE, 2019.

[29] J. Guo and H. Jafarkhani, "Sensor deployment with limited communication range in homogeneous and heterogeneous wireless sensor networks," *IEEE Transactions on Wireless Communications*, vol. 15, no. 10, pp. 6771–6784, 2016.

[30] S. Karimi-Bidhendi, J. Guo, and H. Jafarkhani, "Energy-efficient deployment in static and mobile heterogeneous multi-hop wireless sensor networks," *IEEE Transactions on Wireless Communications*, 2021.

[31] J. Guo and H. Jafarkhani, "Movement-efficient sensor deployment in wireless sensor networks with limited communication range," *IEEE Transactions on Wireless Communications*, vol. 18, no. 7, pp. 3469–3484, 2019.

[32] J. Cortes, S. Martinez, and F. Bullo, "Spatially-distributed coverage optimization and control with limited-range interactions," *ESAIM: Control, Optimisation and Calculus of Variations*, vol. 11, no. 4, pp. 691–719, 2005.

[33] J. Guo, E. Koyuncu, and H. Jafarkhani, "A source coding perspective on node deployment in two-tier networks," *IEEE Transactions on Communications*, vol. 66, no. 7, pp. 3035–3049, 2018.

[34] J. Guo, S. Karimi-Bidhendi, and H. Jafarkhani, "Energy-efficient node deployment in wireless ad-hoc sensor networks," in *ICC 2020-2020 IEEE International Conference on Communications (ICC)*, pp. 1–6, IEEE, 2020.

[35] M. Noori and M. Ardakani, "Design of heterogeneous sensor networks with lifetime and coverage considerations," *IEEE Wireless Communications Letters*, vol. 1, no. 3, pp. 193–196, 2012.

[36] Y. T. Hou, Y. Shi, H. D. Sherali, and S. F. Midkiff, "On energy provisioning and relay node placement for wireless sensor networks," *IEEE Transactions on Wireless Communications*, vol. 4, no. 5, pp. 2579–2590, 2005.

[37] O. Zorlu and O. K. Sahingoz, "Increasing the coverage of homogeneous wireless sensor network by genetic algorithm based deployment," in *2016 Sixth International Conference on Digital Information and Communication Technology and its Applications (DICTAP)*, pp. 109–114, IEEE, 2016.

[38] H. Jafarkhani, *Space-Time Coding: Theory and Practice*. Cambridge University Press, 2005.

[39] M. Haenggi, "Energy-balancing strategies for wireless sensor networks," in *Proceedings of the 2003 International Symposium on Circuits and Systems, 2003. ISCAS'03.*, vol. 4, pp. IV–IV, IEEE, 2003.

[40] W. B. Heinzelman, *Application-specific protocol architectures for wireless networks*. PhD thesis, Massachusetts Institute of Technology, 2000.

[41] S. Lloyd, "Least squares quantization in pcm," *IEEE transactions on information theory*, vol. 28, no. 2, pp. 129–137, 1982.

[42] P. Chatterjee and N. Das, "Multiple sink deployment in multi-hop wireless sensor networks to enhance lifetime," in *2015 Applications and Innovations in Mobile Computing (AIMoC)*, pp. 48–54, IEEE, 2015.

[43] M. Dhami, V. Garg, and N. S. Randhawa, "Enhanced lifetime with less energy consumption in wsn using genetic algorithm based approach," in *2018 IEEE 9th Annual Information Technology, Electronics and Mobile Communication Conference (IEMCON)*, pp. 865–870, IEEE, 2018.

[44] D. R. Dandekar and P. Deshmukh, "Energy balancing multiple sink optimal deployment in multi-hop wireless sensor networks," in *2013 3rd IEEE International Advance Computing Conference (IACC)*, pp. 408–412, IEEE, 2013.

[45] Y. Zou and K. Chakrabarty, "Sensor deployment and target localization in distributed sensor networks," *ACM Transactions on Embedded Computing Systems (TECS)*, vol. 3, no. 1, pp. 61–91, 2004.

[46] B. Paul, *Kinematics and dynamics of planar machinery*. Prentice Hall, 1979.